KINETICS OF CO/CO_2 REACTION WITH MnO_x/TiO_x-CaO-SiO_2 SLAGS

KINETICS OF CO/CO_2 REACTION WITH MnO_x/TiO_x-CaO-SiO_2 SLAGS

By

GARY (YUMING) GAO

A Thesis

Submitted to the School of Graduate Studies

In Partial Fulfilment of the Requirements

for the Degree

Master of Science

McMaster University

Master of Science (2008) McMaster University

Materials Science and Engineering Hamilton, Ontario

TITLE: Kinetics of CO/CO_2 Reaction with MnO_x/TiO_x-CaO-SiO_2 Slags

AUTHOR: Gary (Yuming) Gao, B.Sc. M.Sc., (Northeastern University, China)

SUPERVISOR: Dr. Kenneth S. Coley

NUMBER OF PAGES: xii, 86

ABSTRACT

Knowledge of the interfacial reactions between CO/CO_2 and transition metal oxide containing slags is more important to understand various metallurgical processes. The present research studied the kinetics of reaction between CO/CO_2 and MnO_x/TiO_x containing Slags.

Measurements of the rate of interfacial reaction between CO/CO_2 and MnO_x/TiO_x -CaO-SiO_2 Slags were made using $^{13}CO_2$-CO isotope exchange technique. The dependence of rate constant with respect to the effects of oxygen activity, MnO_x/TiO_x content, slag basicity and temperature was discussed.

It is found that the apparent rate constant increases with increasing MnO_x/TiO_x content, slag basicity and temperature and decreases while increasing oxygen activity. The apparent rate constants obtained for MnO_x/TiO_x containing slags show similar behavior to that of FeO_x containing slags and the rates gradually increase for TiO_x, FeO_x and MnO_x containing slags at same experimental conditions.

The rate constant expressions for MnO_x/TiO_x containing slags are obtained by using a single charge transfer model. Comparison of calculated and measured rate constants shows that there is a good fit between the two, which implies that the single charge transfer model may be generally applicable.

ACKNOWLEDGEMENTS

I am greatly indebted to my supervisor, Dr. Kenneth Coley for his encouragement, guidance and support throughout my years of study. I would like to express my gratitude to him for all I have learnt from him.

I wish to thank the faculty, researchers, staff and graduate students in the Department of Materials Science and Engineering in the course of my study. In particular, I am grateful to Dr. Fuzhong, Ji for his significant help and great ideas in the construction of experimental arrangements. I appreciate the assistance I received from the fellow graduate students, Yi Chen, Judy Li and Elaine Chen.

Lastly, I owe a great deal to my parents and sisters for their enormous encouragements and support. I wish to express my deepest gratitude and love to my wife and my lovely daughter for their love, patience and encouragements.

TABLE OF CONTENTS

LIST OF FIGURES

Chapter 2

Chapter 3

Chapter 4

LIST OF TABLES

Chapter 2

Chapter 3

Chapter 1

INTRODUCTION

With the development of various new smelting and refining process in recent years, there have been numerous studies of the kinetics of gas/slag reactions involving reactive gases. As the presence of transition metal in a slag play a key role in such processes, the knowledge of the interfacial reactions between gases containing CO/CO_2 and transition metal oxide containing slags is more important to understand various metallurgical processes.

In the conventional iron making process, for example, most of the iron oxide is reduced in the solid state, only a small fraction is reduced in the molten slag. In newly developed iron bath smelting processes, such as DIOS and AISI processes, a substantial portion of the iron oxide is reduced in slag by carbon both in solid form and dissolved in the iron bath. The gas/slag interfacial reaction can be also employed in modern electric arc furnaces to increase efficiency of the furnace.[1,2,3] And carbon injection is used in the slag cleaning stage of copper making processes. Due to reduction of magnetite in the slag can lower the slag viscosity, therefore, the content of copper matte in the slag is reduced.[4,5]

Many investigations have been carried out on the kinetics of the reactions between metal oxide containing slag and solid carbon or carbon dissolved in liquid metal. The overall reactions can be expressed as

$$(MO) + C(or\ \underline{C}) = CO + M \qquad [1.1]$$

where $\underline{C}$ denotes dissolved carbon in the liquid metal.

They are typical heterogeneous reactions. As soon as the reaction is initiated by direct contact of carbon and slag, a gas phase, mainly CO and CO_2, is generated, which has been proved by direct observations of reaction through slag by methods such as X-ray fluoroscopy.[6-13] The reaction is then likely to take place via the following two sequential reactions:

$$(MO) + CO = CO_2 + M \qquad [1.2]$$

at the gas/slag interface, and

$$CO_2 + C(or\ \underline{C}) = 2CO \qquad [1.3]$$

at the gas/carbon interface.

There is general agreement[11-16] that several possible rate-controlling processes plus combination of these steps in sequence:

(1) mass transfer of MO_x ($M^{(n+1)+}/M^{n+}$, and O^{2-} ions) from the bulk slag to the gas/slag interface;

(2) reduction of metal oxide in slags by CO on the gas/slag interface, i.e., Reaction [1.2];

(3) mass transfer of CO_2 from the gas/slag interface to the gas/carbon interface;

(4) reaction of CO_2 and solid carbon or carbon in metal on the gas/carbon interface, i.e., Reaction [1.3];

(5) mass transfer of CO from the gas/carbon interface to the gas/slag interface.

To better understand the kinetics of the overall Reaction [1.1], thorough knowledge about the rate of each individual step is needed. Bafghi et al.[17] established models relating slag chemistry to physical properties, which provided possibility to calculate the rate of mass transfer of oxygen in the slag. Other models relating slag properties to the mass transfer coefficient have also been developed.[18,19,20] Calculations of the rate of gas phase mass transfer have shown that the steps (3) and (5) are much faster than the measured overall reaction rate,[11] which means that the gas phase mass transfer is not likely to act as a rate-limiting step.

A number of researchers confirmed that in low iron oxide containing slags, mass transfer of iron oxide, i.e., step (1), is more likely control the overall rate.[12,13,17,21-25] In high iron oxide containing slags, the two interfacial reactions singly or a combination of both reactions may act as the rate-limiting step.[15,18,25] Therefore, among these steps, the two interfacial Reactions [1.2] and [1.3] are very important. The reaction of CO_2 with solid carbon has been the subject of several studies,[26-29] and consistent results were obtained. Recently, a comprehensive study[30] was carried out at temperatures and gas compositions pertinent to bath smelting. The knowledge of carbon gasification is sufficient to re-evaluate the reaction rate in the complex system.[31]

However, knowledge of the rate of the gas/slag interfacial reaction is still inadequate. Numerous studies have been carried out on the kinetics and mechanism of reaction of CO and CO_2 with iron oxide in the slag. Many aspects of the reaction have been studied and empirical relationships have been reported on the dependence of the rate constant on the slag chemistry. Recently, Barati et al.[32-35] gave a detailed description of the reaction kinetics. The dependency of the rate constant of the reaction on four separate variables including temperature, oxygen potential in the gas, iron oxide content in the slag and bulk slag composition were studied, and in turn a comprehensive kinetic model for the reaction was established.

Sun[36] summarized that the apparent first order rate constants obtained for MnO_x and TiO_x containing slags showed similar behavior to that of FeO_x containing slags, but the kinetic data for the reaction between CO/CO_2 and MnO_x/TiO_x containing slags still seems not enough to completely understand the reaction mechanism.

The objectives of this research were to measure the kinetic data for calcium silicate-based slags containing MnO_x and TiO_x and examined the dependence of rate constant on the oxygen activity, chemistry of the melt and temperature. Thus the relationship between the rate constant and the redox ratio (Fe^{3+}/Fe^{2+}, Mn^{3+}/Mn^{2+}, Ti^{4+}/Ti^{3+}) in calcium silicate melts can be obtained. Also the general applicability of Barati's kinetic model will be examined.

Chapter 2

LITERATURE REVIEW

Numerous studies have been carried out on the interfacial reaction kinetics between slag and CO/CO_2 or H_2/H_2O gases, among them Belton and his group conducted a series of studies[37-40] which established the basis for our knowledge of the kinetics and mechanism of such reactions. This chapter attempts to review some of the results of studies on this important topic.

2.1 Rate of Interfacial Reaction between slag and CO/CO_2

The interfacial reaction between slag and CO/CO_2 can generally be written as:

$$CO_{2(gas)} = CO_{(gas)} + O_{(slag)} \qquad [2.1]$$

Most investigators[41-45] have concluded that the reaction follows a first order law with respect to partial pressures of CO and CO_2. Then the rate of Reaction [2.1] can be expressed as:

$$v = \vec{k}P_{CO_2} - \bar{k}P_{CO}a_O \qquad [2.2]$$

where $\vec{k}$ and $\bar{k}$ represent forward and backward rate constants and a_O is the oxygen activity of the melt.

At equilibrium, Equation [2.2] can be written as:

$$v = \vec{k}\left(P_{CO_2} - P_{CO}a_O / K_{eq}\right) \quad [2.3]$$

Where K_{eq} is the equilibrium constant of Reaction [2.1] defined as:

$$K_{eq} = \frac{P_{CO}a_O}{P_{CO_2}} \quad [2.4]$$

Where a_O may be conveniently defined as:

$$a_O = \left(\frac{P_{CO_2}}{P_{CO}}\right)_{eq} \quad [2.5]$$

With the standard state of $a_O = 1$ for a melt in equilibrium with a gas mixture of $P_{CO_2}/P_{CO} = 1$. Equation [2.2] can be written in the form:

$$v = \vec{k}\left(P_{CO_2} - P_{CO}a_O\right) = \vec{k}a_O(P_{CO_2}a_O^{-1} - P_{CO}) \quad [2.6]$$

Generally, the apparent rate constant, k_a, can be correlated to $\vec{k}$ as:

$$k_a = \vec{k}a_O \quad [2.7]$$

Then Equation [2.6] can be rearranged as:

$$v = k_a(P_{CO_2}a_O^{-1} - P_{CO}) \quad [2.8]$$

The apparent rate constant, k_a, has been found to be system and temperature dependent. Because numerous kinetics studies have been concerned with the kinetics of reaction of CO/CO_2 with FeO_x containing slag, the effect of temperature, oxidation state of slag, iron oxide content and slag basicity on the rate constant and mechanism of interfacial reaction between CO/CO_2 and slag are briefly reviewed in the following sections. Similar data on other transition metal oxides (MnO_x and TiO_x) containing slags are also reviewed.

2.2 Dependence of Rate Constant on Slag Composition and Temperature

The redox reaction of iron oxides in slags may be formally written as:

$$(FeO)+0.5CO_2=(FeO_{1.5})+0.5CO \qquad [2.9]$$

According to which the ratio Fe^{3+}/Fe^{2+} may be expressed by

$$Fe^{3+}/Fe^{2+}=K_1(\gamma_2/\gamma_3)(P_{CO_2}/P_{CO})^{0.5} \qquad [2.10]$$

Where K_1 is the equilibrium constant of Reaction [2.9], the γ_2 and γ_3 are activity coefficient of ferrous and ferric ions, respectively, P_{CO_2}/P_{CO} is the oxygen activity, a_O, with standard stated defined as $P_{CO_2}/P_{CO}=1$.

The studies by Sasaki et al.[42] and El-Rahaiby et at.[41] suggested that the apparent first order rate constant for Reaction [2.1], k_a, was almost inversely proportional to the oxygen activity, a_O. This may be expressed as:

$$k_a = k_a^{\circ} a_O^{-\alpha} \qquad [2.11]$$

where k_a° is the value of the rate constant at unit activity of oxygen, $a_O = 1$. k_a° and α in this equation are both dependent on iron oxide content and melt basicity at a given temperature, and α is a constant for a given slag and is close to unity.

Sun et al.[44] confirmed that the slight deviation of α from unity could be attributed to deviations in the dependence of the redox ratio, Fe^{3+}/Fe^{2+}, on the oxygen activity, a_O, from the ideal form of

$$Fe^{3+} / Fe^{2+} \propto a_O^{0.5} \qquad [2.12]$$

The dependence of the apparent rate constant on the redox ratio then can be expressed as

$$k_a = k_a^{\circ} (Fe^{3+} / Fe^{2+})^{-m} \qquad [2.13]$$

Where m is close to 2.

2.2.1 Effect of Iron Oxide Content

Sun[46] and Mori et al. [47] studied the kinetics for low iron oxide containing slags. They showed that increasing iron oxide content up to 30 wt pct did not have a significant impact on the rate. With the increase in iron oxide content from 30 to 100 pct, the rate increases remarkably. At unit molar basicity (CaO/SiO_2=1), a complete range of iron oxide, from zero to 100 wt pct 'FeO' was studied by Barati[48], the dependence can be represented by a second order polynomial function of the form:

$$k_a \propto [\text{'}FeO\text{'}]^2 \qquad [2.14]$$

where $[\text{'}FeO\text{'}]$ is the concentration of iron oxide in wt pct.

The dependence of the apparent rate constant on the iron oxide contend expressed as 'FeO' wt pct is shown in Figure 2.1, k_a increases with iron oxide content with all the experimental conditions.[32]

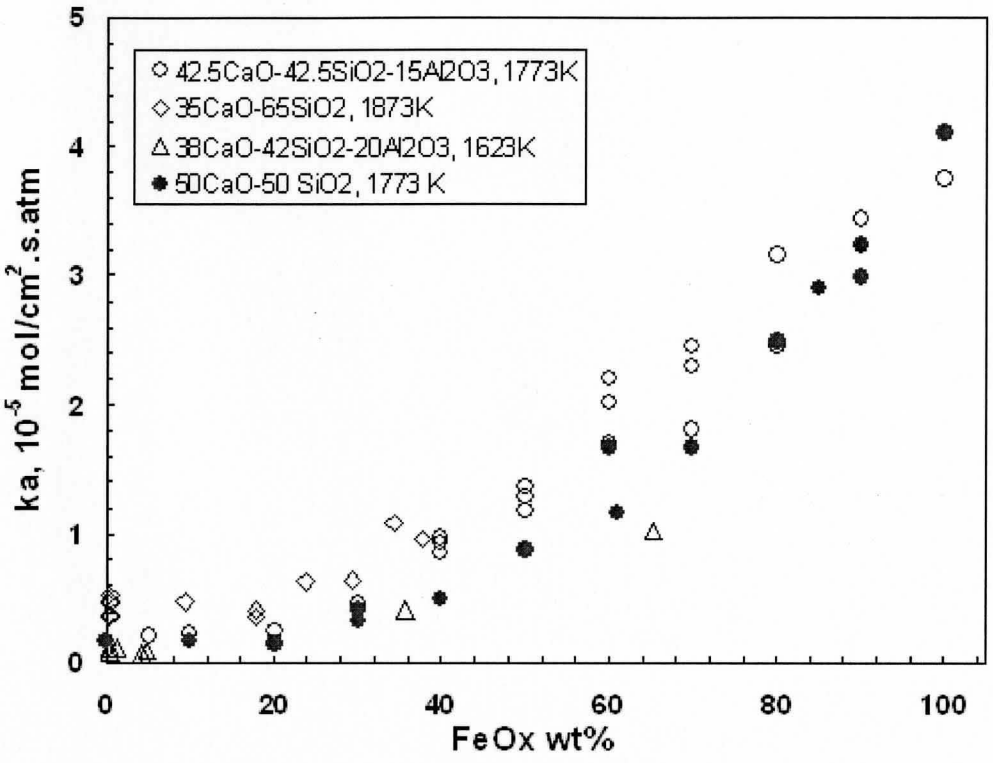

Figure 2.1–Apparent rate constant of oxidation and reduction reaction as a function of iron oxide content, at unit CO_2/CO.[32]

It is may be supposed that at a certain CO_2/CO ratio, increasing FeO content tends to change the Fe^{3+}/Fe^{2+} ratio thereby affecting the rate. Figure 2.2 shows the variation of Fe^{3+}/Fe^{2+} ratio with iron oxide content for some slags[32]. When slag basicity is greater than unity, increasing iron oxide content decreases the redox ratio; on the contrary, the opposite behavior is seen when slag basicity is less than unity. For slags with close to unit basicity, the effect of iron oxide becomes weaker and the redox ratio is essentially independent on the iron oxide content. As stated by Barati[32], the effect of iron oxide content on the redox ratio, therefore, may not be explained without incorporating the effect of bulk slag composition. Also for slags containing less than 10 wt pct FeO,

discrepancies exist on the role of FeO content on the redox ratio. Therefore, the dependence of the rate constant on the iron oxide content can not be related to the changes in the state of oxidation of melt.

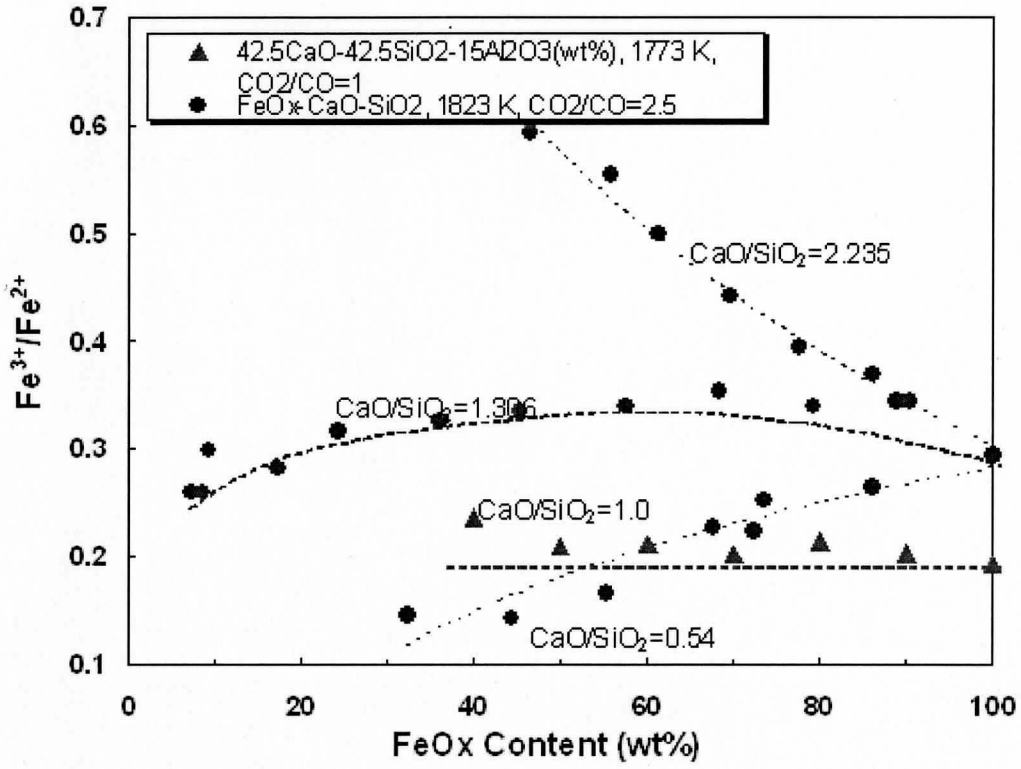

Figure 2.2–Ferric/ferrous ratio as a function of iron oxide content for different slags.[32]

2.2.2 Effect of the Slag Oxidation State

As discussed previously, the apparent rate constant for Reaction [2.1], k_a, was almost inversely proportional to the oxygen activity, a_O, which can be expressed as Equation [2.11]. Figure 2.3 presents the dependence of the apparent rate constant on the CO_2/CO for some melts in logarithmic form. It shows excellent agreement with a linear relationship between log k_a and log (CO_2/CO), and the slopes increase with increasing iron oxide content.[32]

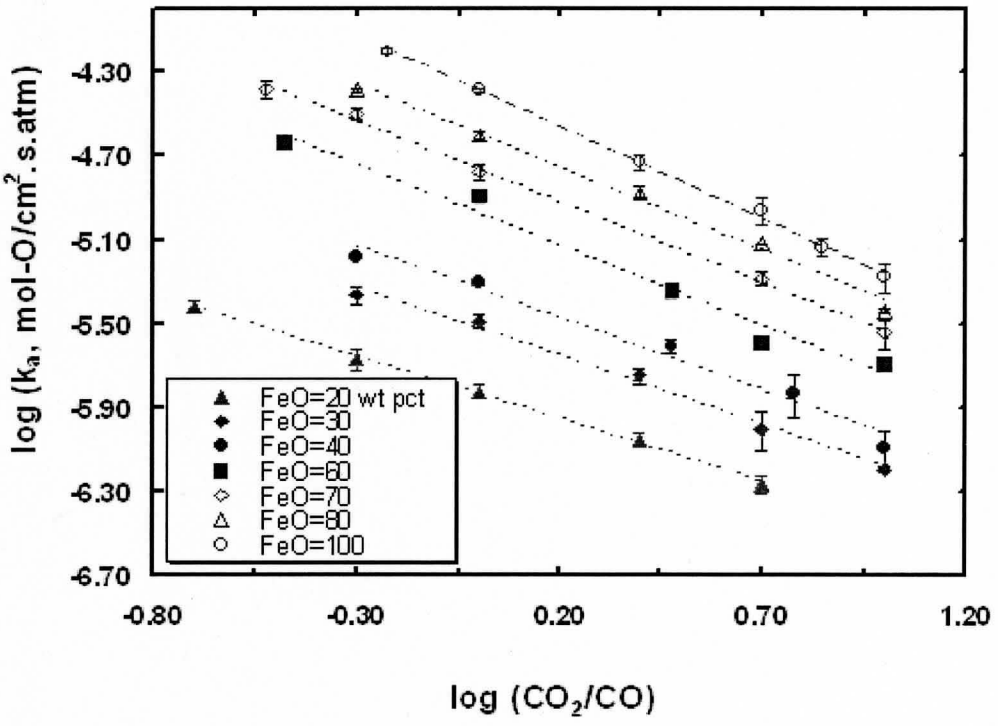

Figure 2.3–Apparent rate constant as a function of the equilibrium CO_2/CO ratio for FeO-CaO-SiO_2(CaO/SiO_2=1, molar ratio) slags, at 1773K.[32]

The value of α is dependent on iron oxide content and melt basicity at a given temperature, ideally, α is equal to 1. It was observed from some studies[42,45,47,49] that the value of α deviated from unity and the extent of deviation varies for different iron oxide contents. Barati et al.[32] found that the values of α started from around 0.5 at low FeO_x containing slags to about 0.9 at iron-rich slags and followed the form

$$\alpha = 0.004 \times \%FeO + 0.5088 \qquad [2.15]$$

The dependence of α on the iron oxide content of the melt is depicted in Figure 2.4.

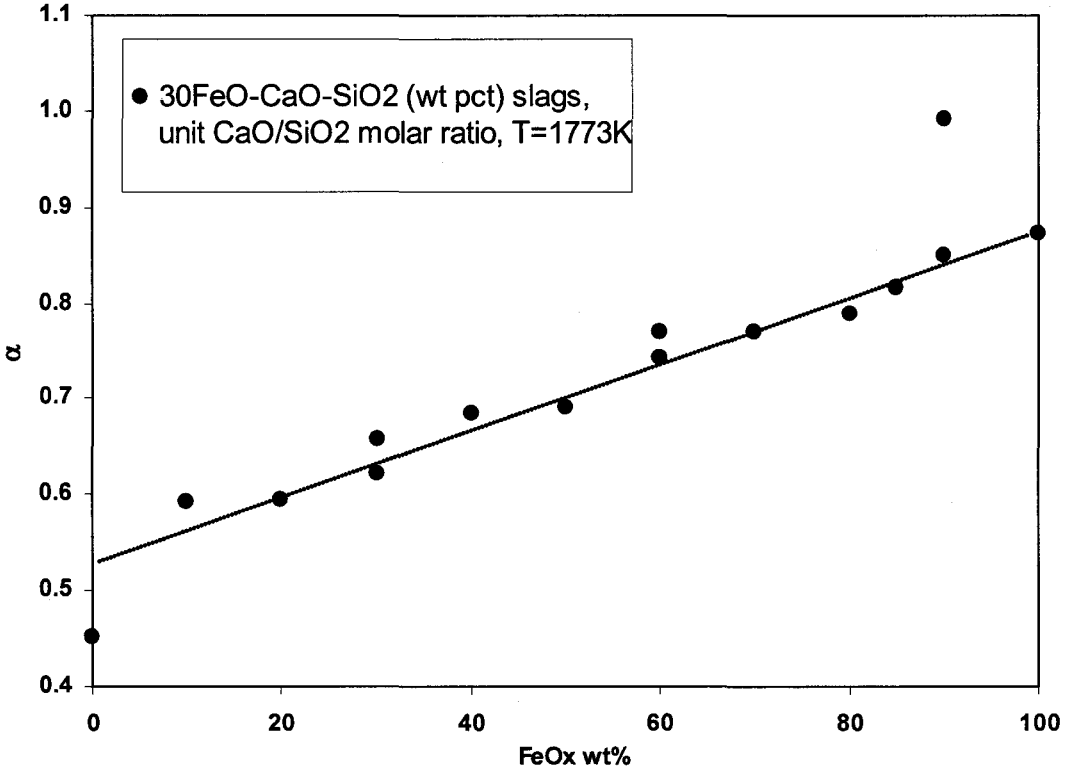

Figure 2.4–Degree of dependence of the apparent rate constant on the oxygen potential, α, as a function of iron oxide content.[32]

2.2.3 Effect of the Slag Basicity

Metallurgical slags are liquid solutions consisting of different oxides, (e.g. CaO, SiO_2, FeO, etc), fluorides (e.g. CaF_2) and sulphides (e.g. CaS) at high temperatures typically above 1200 K. The composites in liquid slags exist in ionic species including cations (e.g. Ca^{2+}, Fe^{2+}, etc.) and anions (e.g. SiO_4^{4-}, PO_4^{3-}, AlO_3^{3-}, etc.). The structure of liquid slag can be described by the effect of metal oxides addition to silica, since most metallurgical slags contain SiO2. The fundamental unit is silicate tetrahedron, SiO_4^{4-} which forms polymeric networks.[50]

The addition of metal oxides (CaO, FeO, etc.) to silica disrupts the silicate network based on the following reaction:

$$-\overset{|}{\underset{|}{Si}}-O-\overset{|}{\underset{|}{Si}}- + MO = -\overset{|}{\underset{|}{Si}}-O^- + {}^-O-\overset{|}{\underset{|}{Si}}- + M^{2+} \qquad [2.16]$$

The size of the silicate units becomes smaller by increasing the MO content, up to the point $MO/SiO_2 = 2$, when each silicon atom forms an individual SiO_4^{4-} tetrahedral.[50]

Most physical and thermodynamic properties of slag, such as the surface tension, electrical conductivity and redox equilibria, are functions of MO/SiO_2 ratio which is known as basicity. Basicity has many different definitions, and conceptually is the free oxygen ion activity. Binary basicity defined by $\frac{(\text{mol\% CaO})}{(\text{mol\% } SiO_2)}$ and optical basicity are mostly used in studies. Optical basicity, Λ, can be expressed as:

$$\Lambda = \frac{\text{Electron Donor Power of Slag}}{\text{Electron Donor Power of CaO}} = \sum_{i}^{n} X_i^* \Lambda_i \qquad [2.17]$$

Where Λ_i is the optical basicity for component I and X_i^* is the mole fraction of component I multiplied by number of oxygen ions in component, for example, 2 for SiO_2.[51]

Many researchers[41,42,45,47,52] have found that the addition of CaO, a basic oxide, to iron oxide increases the rate constant significantly, despite the decrease of the activity of iron oxide. On the other hand, the addition of acidic oxides, such as SiO_2, decreases the rate constant substantially. Li et al.[45] examined the effect of addition of different oxides on the reduction rate of iron oxide, and the result is provided in Table 2.1.

Table 2.1–The apparent rate constant of CO_2 dissociation on different binary systems at CO_2/CO=1.0 and 1773 K. [45]

Slag System	FeO Content (wt pct)	a_{FeO}	Rate Constant (10^5 molO.cm^{-2}.s^{-1}.atm^{-1})
BaO–FeO_x	52.4	0.4	22
CaO–FeO_x	70	0.5	9.8
FeO_x	100	~1	4.1
Al_2O_3–FeO_x	85	0.7	3.3
TiO_2–FeO_x	70	0.7	1.7
	47.37	0.4	1.1
BaO–FeO_x	70	0.5	1

Figure 2.5 shows the dependence of apparent rate constant on the slag basicity, it can be seen that k_a increases approximately exponentially with basicity. The effect of slag basicity on the rate constant may be discussed with regard to its effect on the Fe^{3+}/Fe^{2+} ratio. In Figure 2.2, at fixed oxygen potential, Fe^{3+}/Fe^{2+} increases with slag basicity. According to Equation [2.13], increasing Fe^{3+}/Fe^{2+} ratio leads to decrease the rate, which is contrary to the experimental results.

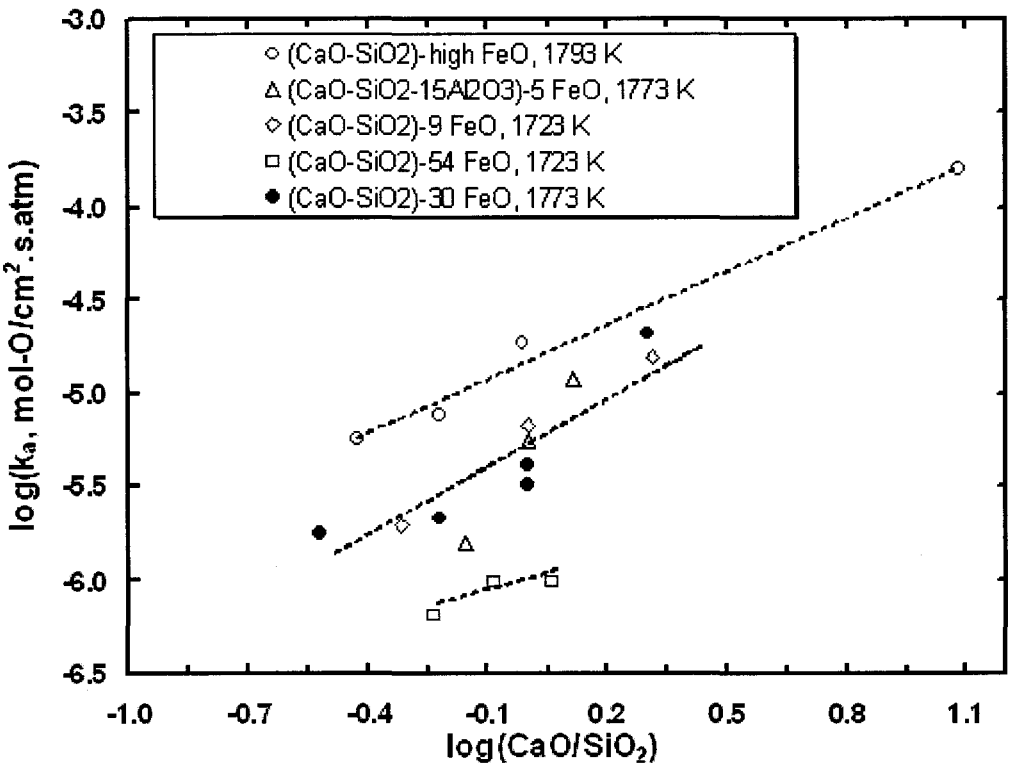

Figure 2.5–Dependence of the apparent rate constant on the slag basicity at unit CO_2/CO (FeO in wt pct).[32]

Another approach to explain the influence of slag basicity on the reaction rate employs the charge transfer mechanism. The addition of basic oxides is expected to result in a higher availability of electrons for the reaction leading to a higher reaction rate. Li and Ratchev[52] found that addition of stronger basic oxides to the iron oxide had more pronounced effect on the reaction kinetics.

Barati et al.[32] studied the dependence of α on slag basicity. The results are plotted in Figure 2.6 and show that increasing the slag basicity has a slight decreasing effect on the value of parameter α. At fixed iron oxide content, the higher the basicity, the less the effect of iron oxide and thus Fe^{3+}/Fe^{2+}. Therefore, higher CaO/SiO_2 weakens that dependency of the rate constant on the Fe^{3+}/Fe^{2+} and oxygen potential, hence α is decreased.

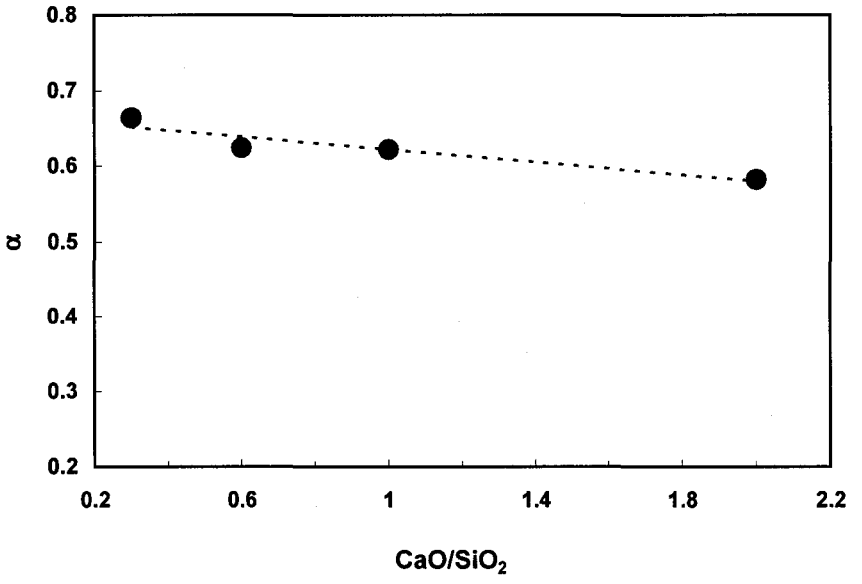

Figure 2.6–Dependence of α on slag basicity at unit CO_2/CO for 30FeO-CaO-SiO_2 (wt pct) slag.[32]

2.2.4 Effect of Temperature

The apparent rate constant follows an Arrhenius relationship with temperature,

$$\log k_a^{\circ} = -E_a / RT + C \qquad [2.18]$$

where E_a is the activation energy of the reaction. The results for some melts examined by Barati et al.[32] are depicted in Figure 2.7. The slope of the Arrhenius plot is essentially constant for all iron oxide content, only the pre-exponential term changes with iron oxide content.

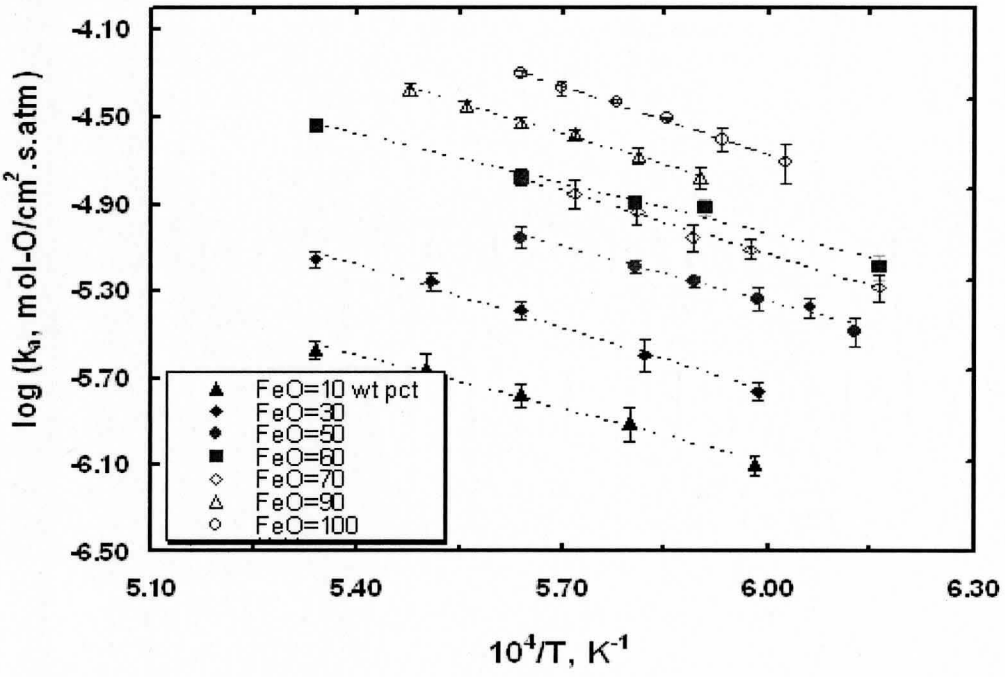

Figure 2.7–Arrhenius plot of the apparent rate constant measured at CO_2/CO=1 for FeO-CaO-SiO_2 (wt pct) slags.[32]

Barati et al.[32] reported that the activation energy at an average value of 178 kJ/mol. In slags with fixed FeO content, increasing the molar basicity of the slag from 0.3 to 2.0 decreases the activation energy from 197 to 146 kJ/mol, which is shown in Figure 2.8. This is in agreement with other findings, showing that addition of basic oxides decreases the activation energy of the reaction.

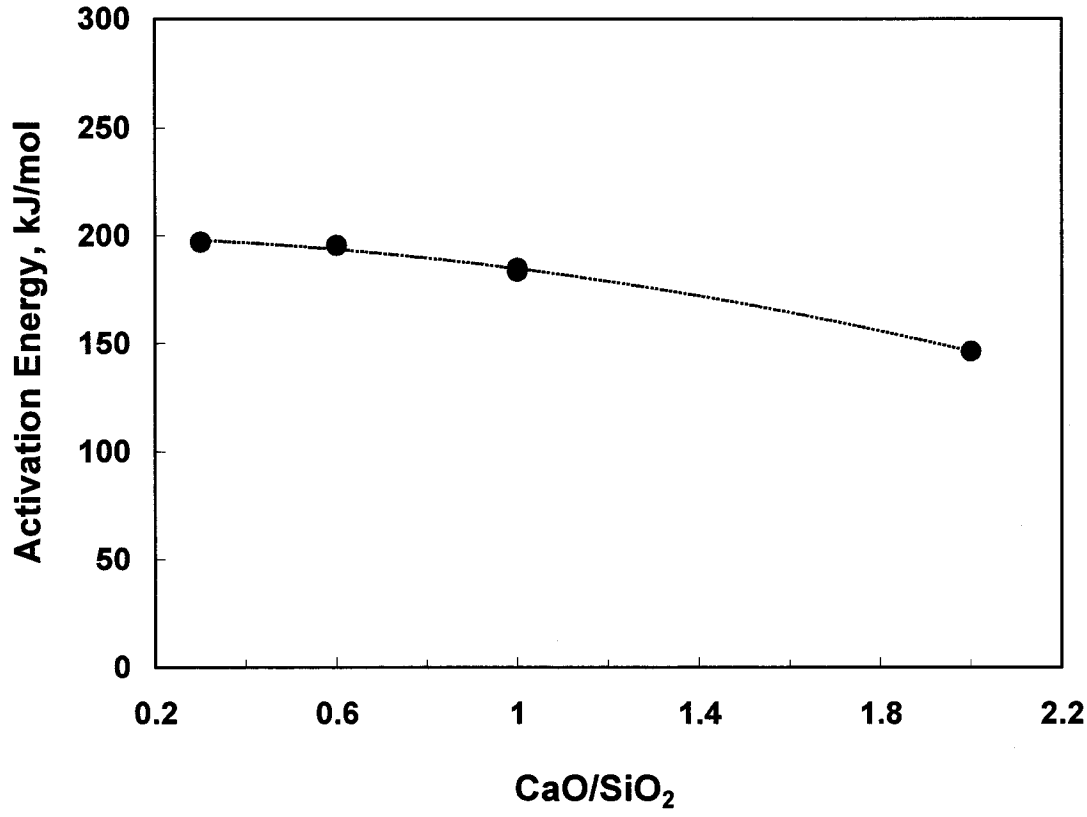

Figure 2.8– Activation energy at unit CO2/CO as a function of binary basicity of the slag, for melts with 30 wt pct 'FeO'.[32]

2.2.5 CO_2/CO Reaction with MnO_x and TiO_x Containing Slags

The rate constants of reactions between TiO_x/MnO_x containing slags and CO_2/CO were found to follow very close behaviors shown in the reactions between FeO_x containing slags and CO_2/CO.

To compare the effect of different transition metals on the rate of gas/slag reaction kinetics, Tran[53] and El-Rahaiby et al.[41] studied the CO_2/CO reaction with manganese oxide containing slags. The rate constant was found to be generally higher than that for iron oxide containing melts at the same oxygen potential and temperature. The first order reduction rate constant for a CaO-MgO-SiO_2 slag with (CaO+MgO)/SiO_2 = 1.2, MgO/CaO = 0.12, and 38 pct 'MnO' was determined with oxygen activity from 30 to 400 at 1400 °C. The results are shown in Figure 2.9. The rate constant is of similar magnitude to that for iron oxide slags but noticeably about two times higher.

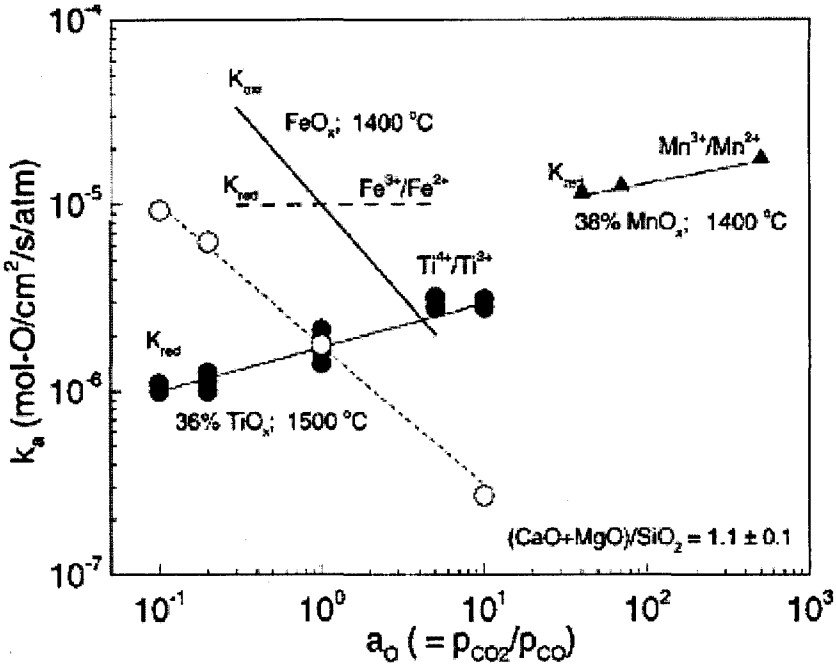

Figure 2.9–Dependence of the apparent rate constant for reduction and oxidation of MnO_x and TiO_x by CO_2/CO gases on the oxygen activity, a_O.[36]

Li[52] investigated the kinetics of reactions between TiO_x containing slags and CO_2/CO gases by a gravimetric method. Some of the results are shown in Figure 2.9. At unit oxygen activity, the rate constant is an order of magnitude lower than that for the reduction of iron oxide from slags with comparable composition. When iron oxide and titanium oxide coexist, the effect of TiO_x on the overall rate of reduction was found to be more complicated. TiO_x acted as a basicity modifier and increased the rate for slags with $CaO/SiO_2 = 0.7$ but decreased the rate for slags with $CaO/SiO_2 = 1.3$.[36]

2.3 Reaction Mechanism

The oxidation or reduction of iron oxide by CO_2/CO must involve the transfer of oxygen to or from the melts. The effect of the slag oxidation state on the rate constant has been discussed in terms of two models; site blockage model presented by Cramb and Belton[55] and charge transfer model by Sasaki et al.[42] Recently, Barati et al.[35] proposed a new kinetic model for the reaction and the rate expression can be applied successfully to calculate the rate constant. These models are described in this chapter.

2.3.1 The Site Blockage Model

The dependence between the reaction rate and the oxygen activity may be correlated with the surface density of the available reaction sites. One may hypothesize that the reaction takes place only on the surface sites unoccupied by adsorbed oxygen atoms or ions. A change in the oxidation state leads to a change of the free adsorption site and, therefore, the rate constant. Cramb and Belton[55] formulated this approach for metal surface and the interpretation of the dependence of the apparent rate constant on oxygen activity by this consideration is referred as the site blockage model.

Considering the equilibrium,

$$CO_{2(g)} = CO_{(g)} + O_{(ad)} \qquad [2.19]$$

The rate constant for the reaction may be written as:

$$k_a = k_f(1-\theta_O) \qquad [2.20]$$

where k_f is the rate constant of the forward reaction for the dissociation of CO_2 at the bare melt surface and θ_O is the fractional coverage by the adsorbed oxygen.

Assuming an ideal Langmunir adsorption, θ_O may be written as:

$$\frac{\theta_O}{1-\theta_O} = K_O a_O \qquad [2.21]$$

Or

$$(1-\theta_O) = \frac{1}{1+K_O a_O} \qquad [2.22]$$

Where K_O is the adsorption coefficient of oxygen with respect to the CO_2/CO ratio.

Combining Equations [2.20] and [2.21],

$$\frac{1}{k_a} = \frac{1}{k_f} + \frac{K_O}{k_f} a_O \qquad [2.23]$$

It suggests that k_a must decrease with a_O, which is accordance with the Equation [2.11]. Cramb and Belton[55] concluded that the dependence of the apparent rate

constant on the CO_2/CO ratio is consistent with surface blockage by oxygen with ideal Langmuirian adsorption essentially up to liquid oxide formation.

As discussed before, the addition of basic oxide to iron oxide increases the rate constant significantly, despite the decrease of the free adsorption sites. In many cases, it is not sufficient to just consider the effect of the site blockage, and the charge transfer model must be employed.

2.3.2 The Charge Transfer Model

Molten slag is a mixture of different ions. Transition metals, such as iron and titanium, no matter what their exact forms are, exist as ions in slags. The reduction of oxidation of iron and titanium in slag from one valence to another inevitably involves the transfer of charge. The oxygen in slag is also not a neutral atom but an electrically charged ion, the transfer of oxygen must involve intermediate, adsorptive, charged radicals on the surface of the slag. A change in the oxidation state generally leads to a change of concentration of excess electrons. [56] The dependence of the apparent rate constant on the oxygen activity may therefore be explained by the charge transfer effects, and the interpretation of the dependence by charge transfer consideration is referred to as the charge transfer model.

Sasaki et al.[42] in their model proposed a mechanism involving the transfer of two electrons as follows. Considering redox equilibra as the form:

$$CO_{2(ad)} + 2Fe^{2+} \rightarrow CO^{2-}_{2(ad)} + 2Fe^{3+} \qquad [2.24]$$

For a given number of reaction sites, at equilibrium the surface concentration of weakly adsorbed CO_2^{2-} ions, $\Gamma_{CO_2^{2-}}$ was obtained as

$$\Gamma_{CO_2^{2-}} \propto P_{CO_2}\left(Fe^{2+}/Fe^{3+}\right)^2 \qquad [2.25]$$

Assuming one of the following reactions involving the transfer of two charges as the rate determining step,

$$CO_{2(ad)} + 2e^- \rightarrow CO_{2(ad)}^{2-} \qquad [2.26]$$

$$CO_{2(ad)}^{2-} \rightarrow CO + O^{2-} \qquad [2.27]$$

In either case, the rate law for the forward reaction is expressed by:

$$\vec{v} = k_a^{\circ} P_{CO_2}\left(Fe^{2+}/Fe^{3+}\right)^2 \qquad [2.28]$$

Substitution Equation [2.12] into Equation [2.28],

$$\vec{v} = k_a^{\circ} P_{CO_2}\left(P_{CO_2}/P_{CO}\right)^{-1} \qquad [2.29]$$

Therefore,

$$k_a = k_a^{\circ} a_O^{-1} \qquad [2.30]$$

The value of $\alpha = 1$, obtained from this model was thought to be consistent with the experimental observation by Sasaki et al.[42]

However, the results from some other studies[45,49] showed that the value of α slightly deviated from unity. Barati[45] suggested that the small deviation from ideal behavior predicted by the charge transfer model may be explained as follows:

(a) The surface constitution of the melts may change with variation in the oxidation state. The above equations are derived for a given reaction site, however, the number of reaction sites may change with oxidation state. The small deviation from ideal behavior may be from a small interference by the effect of site blockage.

(b) Transfer of two charges is not the rate determining step of the overall reaction. The value of $\alpha = 1$ in the charge transfer model has been obtained upon the assumption that transfer of two charges from slag to the adsorbed CO_2 is the rate–determining step. Assuming that the iron redox equilibria behaves 'ideal' in redox equation

$$(Fe^{2+}/Fe^{3+}) \propto (\gamma_3/\gamma_2).(CO/CO_2)^{0.5} \qquad [2.31]$$

Where γ_3/γ_2 remains constant the examined range of oxygen potential.

If the ratio of γ_2/γ_3 depends on the oxidation state of the slag, the redox equilibria can be approximated by the relationship as[57-61]:

$$Fe^{3+}/Fe^{2+} \propto (CO_2/CO)^{\beta} \qquad [2.32]$$

Where the value of β differs from 0.5, the ideal value. Table 2.2 shows some

values of α and 2β for various melts compiled by Barati[48]. For some slags, the close relationship of $\alpha = 2\beta$ is followed; however, for many other experimental conditions, the relationship is not obeyed, and the value of α mostly are between 0.5 and 1. It may be concluded that the deviation of γ_2 / γ_3 from unity may not be the only reason for which dependence of the rate constant on oxygen activity deviates from ideal behavior.

Table 2.2– Degree of dependence of the apparent rate constant (α) and Fe^{3+}/Fe^{2+} (β) on the equilibrium oxygen potential.[48]

Slag	α	2β
Pure FeO_x	1.05 (at 1693 K) 0.9 (at 1773 K) 0.8 0.87	1.0
Calcium ferrite (24 mol pct CaO)	0.79	0.83
Equimolar $CaO–SiO_2–FeOx$	0.75	0.68 0.80
Silica saturated iron silicate	1.0	1.0
$CaO–SiO_2$–5 wt pct FeO, (CaO/SiO_2)=1	0.84	0.9

The double charge transfer model explained some of the relationships between the apparent rate constant and experimental variables, but failed to explain the deviation of the value of α from unity. Barati et al.[35] modified the charge transfer model by assuming that a single charge transfer is the rate–determining step, and developed a

mathematical model on the basis of this mechanism to present a quantitative relationship of the dependence of the apparent rate constant on the experimental parameters.

2.3.3 The Single Charge Transfer Model

Considering the overall oxidation reaction of FeO in liquid slag by CO_2 in ionic form as:

$$2Fe^{2+} + CO_2 = 2Fe^{3+} + O^{2-} + CO \qquad [2.33]$$

In the single charge transfer model by Barati et al.[35], the reaction can be broken into the following elementary steps:

(1) the adsorption of CO_2 on the surface of the melt;

$$CO_{2(g)} + \square = CO_{2(ad)} \qquad [2.34]$$

Where the symbol $\square$ represents a suitable site for adsorption of CO_2.

(2) the donation of electron s by the ferrous/ferric redox couple;

$$Fe^{2+} = Fe^{3+} + e^- \qquad [2.35]$$

(3) single charge transfer;

$$CO_{2(ad)} + e^- \rightarrow CO_{2(ad)}^- \quad [2.36]$$

(4) the dissociation of charged radicals;

$$CO_{2(ad)}^- + e^- = CO_{(ad)} + O^{2-} \quad [2.37]$$

(5) the desorption of CO to the gas phase;

$$CO_{(ad)} = CO_{(g)} \quad [2.38]$$

The single charge transfer is the rate determining step and the rate can be expressed as

$$v = k\Gamma_{CO_{2(ad)}}\left(a_{e^-}\right) \quad [2.39]$$

Where $\Gamma_{CO_{2(ad)}}$ is the concentration of weakly adsorbed CO_2, a_{e^-} is the activity of free or quasi–free electrons.

$\Gamma_{CO_{2(ad)}}$ is in proportion to the square of the concentration of Fe^{2+},

$$\Gamma_{CO_{2(ad)}} \propto \left(C_{Fe^{2+}}\right)^2 \quad [2.40]$$

because a suitable site for adsorption of CO_2 must essentially be located between two ferrous sites and Fe^{2+} plays two roles in the reaction; providing an electron for the formation of charged activated complexes and coordinating with the resulting oxygen ion in the final melt structure. In case of other sites, there will be mass transport in which the electron moves to the reaction site and oxygen ion diffuses to the position between Fe^{3+}, which either must be very fast or the interfacial reaction will not be the

rate determining step.

For the attachment of electrons to the adsorbed gas, the electrons first must be free and overcome the energy gap. Wolkenstein[62] correlated the activity of free electron and the energy gap as

$$a_{e^-} = k' \exp\left(\frac{-\Phi}{\kappa T}\right) \qquad [2.41]$$

Where κ is the Boltzman constant and Φ represent the energy gap. Φ is given by

$$\Phi = E_C + \Phi_S - E_F \qquad [2.42]$$

Where E_C is conduction band energy, E_F is Fermi energy and Φ_S is surface potential.

Reiss[63] employed a nernst type equation to express E_F as a function of redox couple Fe^{2+}/Fe^{3+},

$$E_F = E^\circ + \kappa T \ln\left(\frac{\gamma_3[Fe^{2+}]}{\gamma_2[Fe^{3+}]}\right) \qquad [2.43]$$

Where E° is the Fermi level at standard state and a function of temperature only.

All the energy terms are ultimately gathered in the apparent activation energy (E_a) as

$$E_a = E + E_\Lambda \qquad [2.44]$$

Where E is a constant and E_Λ is a function of the optical basicity of the slag. The addition of basic oxide brings about several effects on the energy levels. At a fixed oxygen potential, increasing the basicity increases the activity of oxygen, thereby E_F is displaced to higher levels. On the other hand, it will decrease E_C with decreasing the density of negative charges on the surface.[35]

The final form of the rate constant expression is presented as

$$k_a = k^\circ \left(C_{Fe}\right)^2 \frac{1}{r(1+r)^2} \exp\left(\frac{-E_a}{RT}\right) \qquad [2.45]$$

Where k° can be regarded as a global constant for the reaction, C_{Fe} is the total iron concentration in the bulk in molar percent, r is the ratio of Fe^{3+}/Fe^{2+}, R is the gas constant. As for $CaO–SiO_2–FeO_x$ system, the quantitive form of the rate constant is given by

$$k_a = 2.67\times10^{-4} \left(C_{Fe}\right)^2 \frac{1}{r(1+r)^2} \exp\left(\frac{-(475.7-452.4\Lambda)}{RT}\right) \qquad [2.46]$$

The comparison between calculated values and experimental rate constants is shown in Figure 2.10.[35]

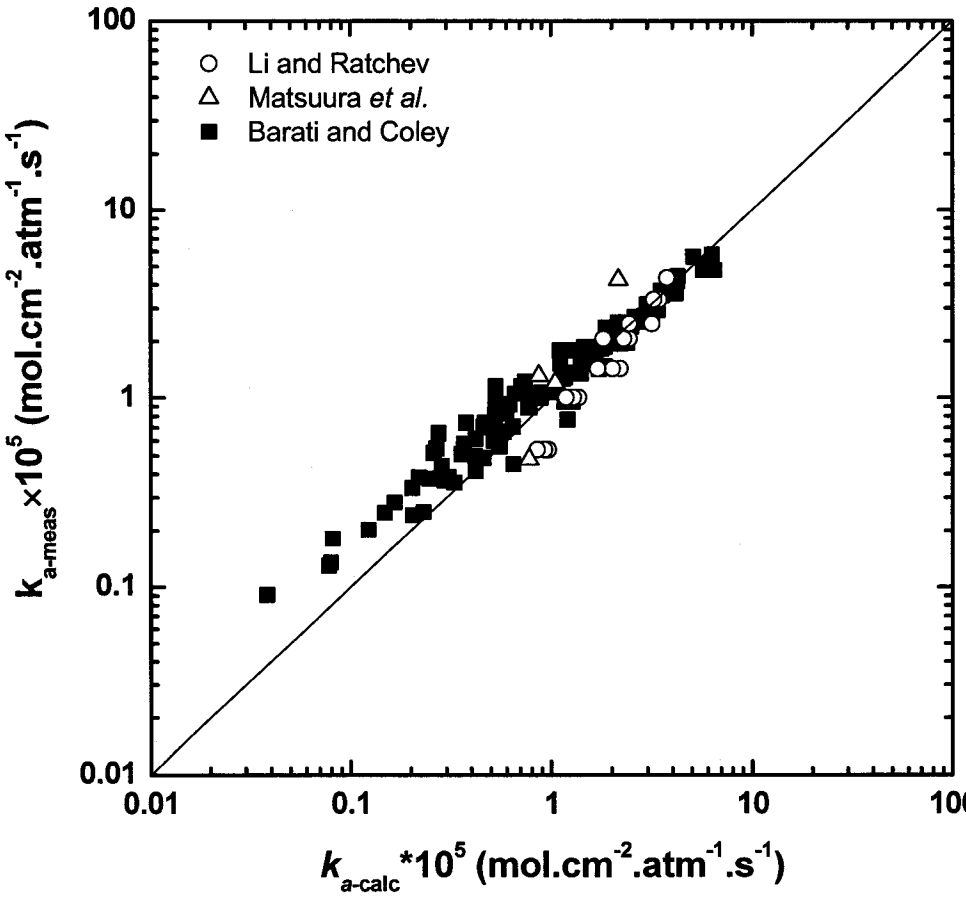

Figure 2.10–Comparison between calculated and measured rate constants under various experimental conditions.[35]

Chapter 3

EXPERIMENTAL PROCEDURES

3.1 Experimental Techniques

There are typically two predominant methods to be used to measure the rate of interfacial reactions between CO_2/CO and slags. One is the gravimetric method.[45,52] The melt is pre-equilibrated with the mixtures of desired CO_2/CO ratio and then reacted with a more oxidizing or reducing gas mixture in non–equilibrium conditions, the rate of weight change of the sample is measured and used to calculate the rate constant of reduction/oxidation reaction.

Another method is isotope exchange method, which has been widely used in the determination of reaction paths and the rates of elementary steps in the heterogeneous catalysis of gas reactions. Grabke first used the isotope exchange method to study high temperature metallurgical reactions.[64,65] Later, Belton and his associates extended the application of the technique to the kinetic studies of interfacial reactions between CO_2/CO and different slags.[41-44,47] The major advantage of the isotope exchange technique is that the rate measurement is carried out under chemical equilibrium conditions and the effect of condensed phase mass transfer is irrelevant, the measured rate constant, therefore, can be regarded as the true interfacial rate constant. The isotope exchange technique was used in the present study.

3.2 Isotope Exchange Method

In the isotope exchange technique, after the CO_2/CO mixture and melt are equilibrated for sufficiently long time, labeled (isotope) gas $^*CO_2$ is introduced to the gas flow. The flowrates are adjusted to keep the total CO_2/CO ratio constant before and after addition of isotope gas. Therefore, the equilibrium state remains unchanged and the net oxygen transfer between gas and melt is zero. The overall exchange reaction is given by

$$^*CO_{2(g)} + {}^{12}CO_{(g)} = {}^*CO_{(g)} + {}^{12}CO_{2(g)} \qquad [3.1]$$

Where the labelled carbon isotope indicated by *, can be either the radioisotope ^{14}C or stable isotope ^{13}C.

Since the natural CO_2 contains negligible concentration of $^{14}CO_2$ radioisotope, Cramb et al.[66] employed the following equation to determine the apparent rate constant of CO_2 dissociation when $^{14}CO_2$ is the tracer isotope:

$$\frac{\overset{\circ}{V}}{ART}\frac{1}{1+\beta}\ln\left[\frac{1}{1-P_{^{14}CO}/(P_{^{14}CO})_{eq}}\right] = \bar{k}_a \qquad [3.2]$$

where A is the reaction area (cm^2), R is the gas constant (cm^3 atm mol^{-1} K^{-1}), T is the absolute temperature (K), β is the equilibrium CO_2/CO ratio, $\overset{\circ}{V}$ is the volume flow rate of the gas mixture (cm^3 s^{-1}), $P_{^{14}CO}$ is the partial pressure of tagged CO in the reacted gases, $(P_{^{14}CO})_{eq}$ is the partial pressure of labeled CO in the isotopic

equilibrium condition, and $\vec{k}_a$ (mol O cm^{-2} s^{-1} atm^{-1}) is the apparent rate constant of the forward reaction..

When employing $^{13}CO_2$ in the experiments, because ^{13}C has a significant natural abundance (~ 1.1%), the natural ^{13}C concentration can not be neglected. The use of Equation [3.2] for ^{13}C would introduce some error, and it should be modified by taking into account the natural abundance of ^{13}C.

The overall exchange reaction with ^{13}C being the tracer isotope can be written as:

$$^{13}CO_2 + {}^{12}CO \leftrightarrow {}^{13}CO + {}^{12}CO_2 \qquad [3.3]$$

The first-order rate of $^*CO_2$ dissociation per unit area can be expressed as

$$\frac{dn_{*CO}}{dt} = \vec{k}(1-\Sigma\theta_i)P_{*CO_2} - \overleftarrow{k}P_{*CO}\theta_O \qquad [3.4]$$

where θ_i represents the fractional coverage of adsorbed species i which can prevent dissociation of CO_2 by adsorption on reaction sites, θ_O is the fractional coverage by oxygen, n is number of moles, P represent partial pressure of gases, and $\vec{k}$ and $\overleftarrow{k}$ are the forward rate constant and the reverse rate constant, respectively.

When Reaction [3.3] gets equilibrium,

$$\left(\frac{P_{^{13}CO_2}}{P_{^{13}CO}}\right)_{eq} = \left(\frac{P_{CO_2}}{P_{CO}}\right)_{eq} = \frac{\vec{k}\theta_O}{\vec{k}(1-\Sigma\theta_i)} = \beta \qquad [3.5]$$

For ideal gas, PV=nRT, rearranging Equation [3.4] and obtain

$$\frac{V}{ART}\frac{dP_{^{13}CO}}{dt} = \vec{k}(1-\Sigma\theta_i)\left[P_{^{13}CO_2} - P_{^{13}CO}(P_{CO_2}/P_{CO})_{eq}\right] \qquad [3.6]$$

Conservation of isotope ^{13}C gives

$$P^{\circ}_{^{13}CO_2} + P^{\circ}_{^{13}CO} = P_{^{13}CO} + P_{^{13}CO_2} \qquad [3.7]$$

Where $P^{\circ}_{^{13}CO}$ is the partial pressure of natural ^{13}CO and $P^{\circ}_{^{13}CO_2}$ is the partial pressure of $^{13}CO_2$ isotope in ingoing CO_2.

At equilibrium,

$$P^{\circ}_{^{13}CO_2} + P^{\circ}_{^{13}CO} = (P_{^{13}CO})_{eq} + (P_{^{13}CO_2})_{eq} = (P_{^{13}CO})_{eq}(1+\beta) \qquad [3.8]$$

Substituting Equations [3.5] and [3.7] to Equation [3.6],

$$\frac{V}{ART}\frac{dP_{^{13}CO}}{dt} = \vec{k}(1-\Sigma\theta_i)\left[P^{\circ}_{^{13}CO_2} + P^{\circ}_{^{13}CO} - P_{^{13}CO}(1+\beta)\right] \qquad [3.9]$$

According to the conditions that (t = 0 , $P_{13_{CO}} = P^{\circ}_{13_{CO}}$) and (t = t, $P_{13_{CO}}$), we obtain

$$\frac{V}{ART}\frac{1}{1+\beta}\ln\left[\frac{P^{\circ}_{13_{CO_2}} + P^{\circ}_{13_{CO}} - P^{\circ}_{13_{CO}}(1+\beta)}{P^{\circ}_{13_{CO_2}} + P^{\circ}_{13_{CO}} - P_{13_{CO}}(1+\beta)}\right] = \vec{k}(1-\Sigma\theta_i)t \qquad [3.10]$$

Substituting Equations [3.8] to Equation [3.10], the final form of expression of rate constant is

$$\frac{\dot{V}}{ART}\frac{1}{1+\beta}\ln\left[\frac{1-P^{\circ}_{13_{CO}}/(P_{13_{CO}})_{eq}}{1-P_{13_{CO}}/(P_{13_{CO}})_{eq}}\right] = \vec{k}_a \qquad [3.11]$$

Where $\vec{k}_a$, apparent rate constant of forward reaction, equals to $\vec{k}(1-\Sigma\theta_i)$, and $\overset{\circ}{V}$ = V/t, which is volume flow rate of gas mixture.

3.3 Experimental Arrangements

3.3.1 Experimental Materials

There are four gases used in the experiments, CO_2, CO, $^{13}CO_2$ and Ar. CO_2, CO and Ar were supplied from Air Liquid Inc. and all had initial purities of 99.5 pct. $^{13}CO_2$ was produced by Icon Isotopes Inc., USA and was supplied in 50 L cylinders.

Slag samples were made from high purity, reagent grade powders of CaO, SiO_2, Fe_2O_3, MnO_2 and TiO_2. Their properties are provided in Table 3.1.

Table 3.1– Properties of slag making materials.

Material	Purity (wt pct)	Size	Supplier
CaO	96 (3.3 % LOI)		Fisher Chemicals
SiO_2	99.5	–400 mesh	Alfa Aesar
MnO_2	99.9		Alfa Aesar
TiO_2	99.5		Alfa Aesar
Fe_2O_3	99.8	–325 mesh	Alfa Aesar

Two kinds of platinum crucibles were used in this study. As for the crucible size, the inner diameters were same for each case, all were 11mm; the heights were different, one was 12mm for preliminary experiments and another was 8mm for the main experiments.

3.3.2 Experimental Setup

The experimental setup is same as that used in Barati's study, and is shown in Figure 3.1.[48] CO, CO_2 and $^{13}CO_2$ gases were first passed through digital mass flow controllers. Flow controllers were operated by DFC software installed on a PC. All flow controllers were calibrated before each experiment using a soap bubble flowmeter.

After passing through flow controllers, gases came into drying columns filled with Drierite and silica gel. CO was passed through an additional Ascarite column to strip out any traces of CO_2.

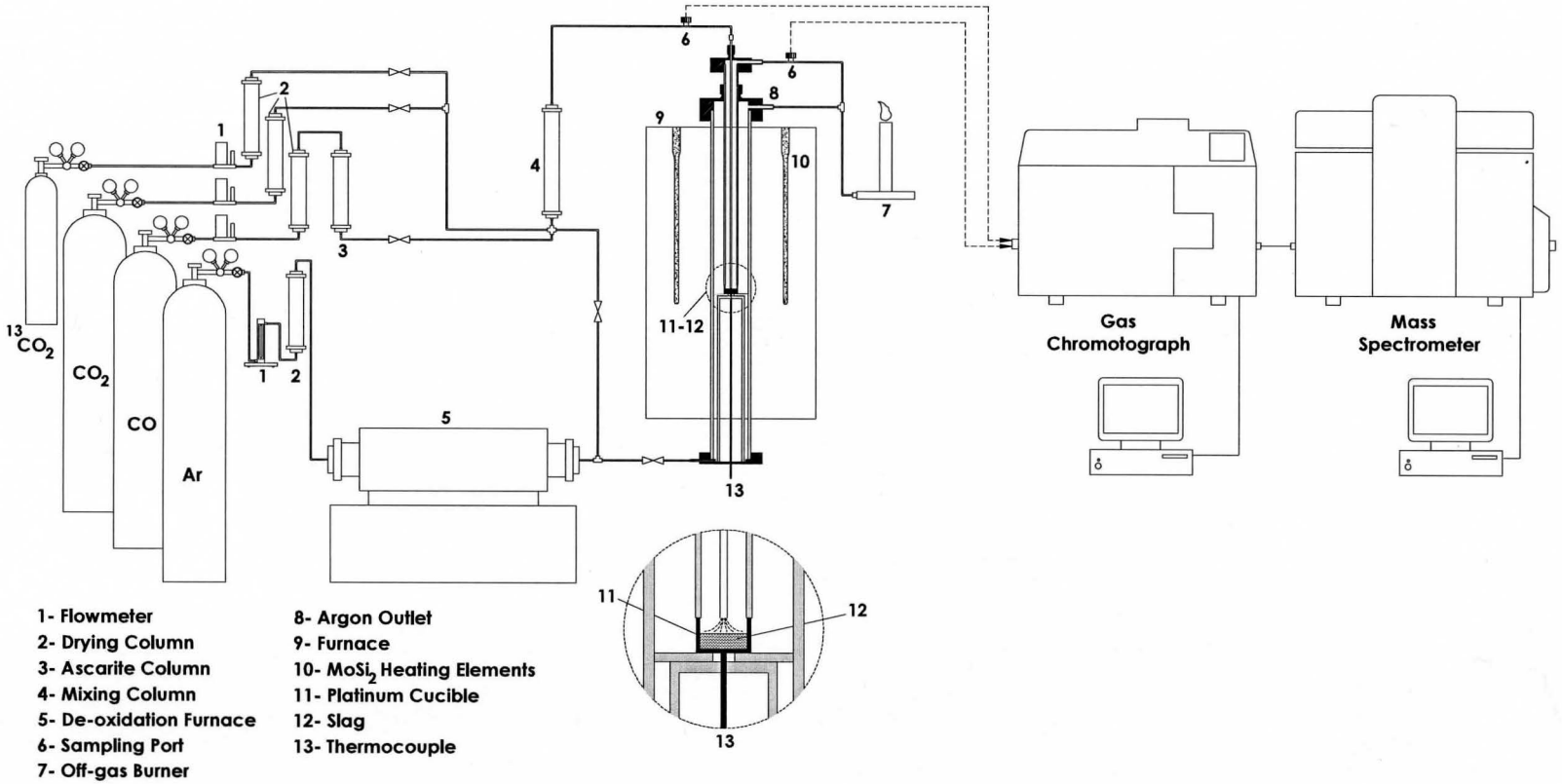

Figure 3.1– Schematic diagram of the experimental arrangement in kinetic measurements.[48]

A separate argon flow was used to seal the inner tube of the furnace from air. The flowrate of Argon was adjusted by a direct reading flow controller. Before entering into the furnace, Argon passed through Drierite column and a furnace containing copper at 500–600 °C to remove moisture and oxygen.

The high temperature experiments were carried out in a furnace with 4 U–shape $MoSi_2$ as heating elements. An alumina working tube with inner diameter 80mm was used to heat the slag. Both the top and bottom of the working tube were sealed with an water-cooled stainless steel caps. A crucible containing slag sample and reaction tube were placed inside the working tube, and a type B thermocouple (Pt–6 pct Rh/Pt–30 pct Rh) inserted from the bottom was located near the crucible. Temperature was controlled automatically by a programmable EUROTHERM Controller. A temperature variation of ±1°C was measured in a zone approximately 40 mm in height. During all experiments the reaction crucible was placed in this zone. The temperature profiles in the working tube were shown in Figure 3.2.

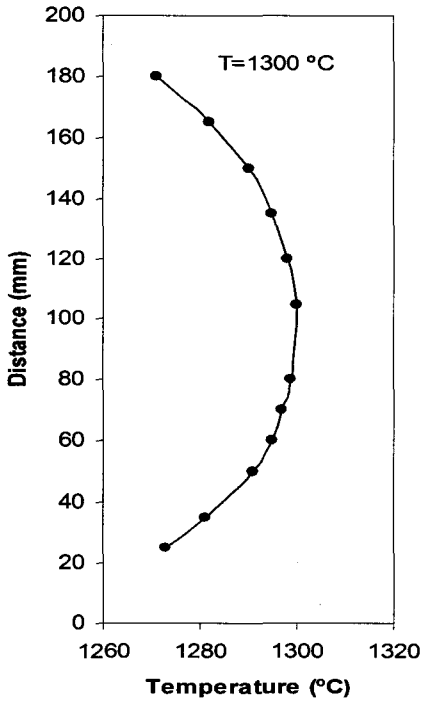

Figure 3.2–The temperature profile of the furnace (set temperature =1300 °C)

The whole system was sealed and Argon was passed through the working tube to prevent air ingress into the reaction tube. Figure 3.3[32] shows the detailed arrangement inside the furnace.

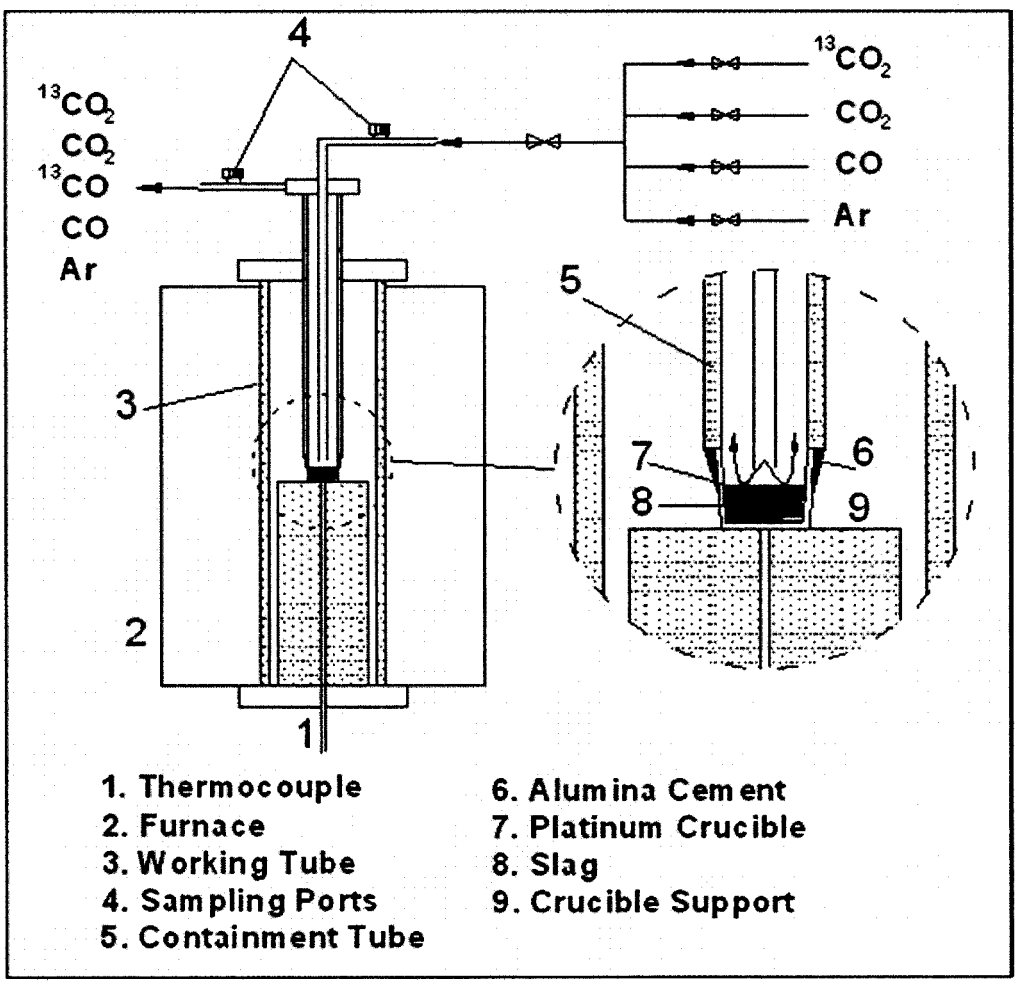

Figure 3.3–Schematic diagram of the experimental setup.[32]

A gas chromatograph (XL GC, Perkin Elmer) and An isotope ratio mass spectrometer (Isoprime, Micromass, UK) were used to analyze the gas sample. Each gas mixture sample first was injected into GC, in which it was separated and a pure CO_2 gas sample was sent to mass spectrometer (MS). The concentration of $^{13}CO_2$ in CO_2+$^{13}CO_2$ mixture is then measured in the MS and used in calculating the rate constant.

3.3.3 Experimental Procedures

A slag sample weighing about 0.5-1.0 gram was loaded into the crucible, which was attached to the reaction tube by alumina cement. The crucible and the attached tube were placed in the hot zone inside the working tube and the temperature was raised to the target temperature gradually while Argon flowed through the working tube.

Once the desired temperature was achieved, a CO_2/CO gas mixture was introduced by an alumina tube (ID=5mm) to within 5 mm of the surface of the melt. Flowrate controllers were adjusted to yield the preferred CO_2/CO ratio and total flowrate. After the gas mixture and slag achieved equilibrium in approximately an hour, the labeled gas was introduced. The gas samples for analysis were taken after 15 minutes when the isotope exchange reaction reached steady state.

3.4 Preliminary Results

3.4.1 Estimation of the Equilibrium time

Because the isotope exchange method is conducted at gas/slag reaction equilibrium, experimental time must be long enough to achieve equilibrium. By comparing the ratio of CO_2/CO in ingoing and outgoing gas, the equilibrium time can be determined.

In the experiment for determination of the equilibrium time, the CO_2/CO ratio was set as 1.0 with a 200 mL/min flowrate, the slag sample was 2.0 grams $30TiO_2$-35CaO-$35SiO_2$ (wt pct) slag. Compared the conditions in the main experiments, the

equilibrium time should be longer than that of main experiments. The outgoing gas composition was measured by GC and is plotted as a function of time in Figure 3.4. It shows that after 40 minutes, the CO_2/CO ratios are almost same in the ingoing and outgoing gases, which implies that the equilibrium has been achieved. Therefore, the labeled gas was introduced after an hour in all subsequent experiments.

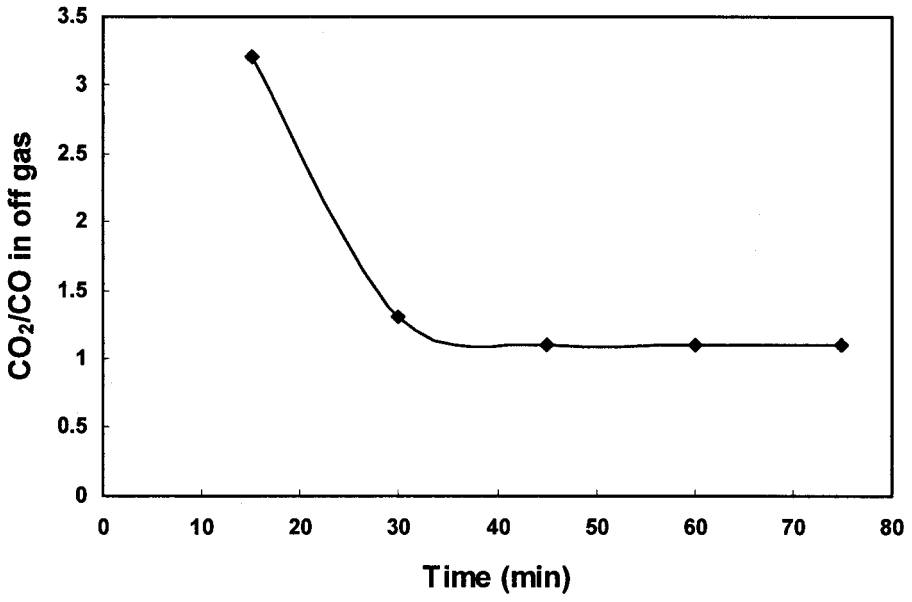

Figure 3.4–CO_2/CO ratio in off–gas as a function of time for 30TiO_2-35CaO- 35SiO_2 (wt pct) slag with CO_2/CO=1.0 (T= 1773 K and flowrate = 200 mL/min).

3.4.2 Optimum Gas Flowrate

In order to measure the rate of gas/slag interfacial reaction, the rate of mass transport in either gas phase or slag phase must be eliminated. Because the reaction is in equilibrium, the net oxygen transfer between gas and slag is zero, therefore there is no net mass transfer in the slag. There must be an optimum gas flowrate, which is high enough to minimize the effect of mass transfer control in the gas phase and to be not too high to cause a significant change in the interfacial reaction area, which leads to reducing the precision of the method.

To find the optimum gas flowrate, the total flowrate of gases was varied between 200 to 700 mL/min with unit CO_2/CO ratio in $30TiO_2$-35CaO- $35SiO_2$ (wt pct) slag. The results are shown in Figure 3.5. It shows that the rate constant became independent of flowrate when the flowrate was above 450 mL/min. Therefore, the total flowrate was kept in 500 mL/min to ensure the interfacial chemical control regime.

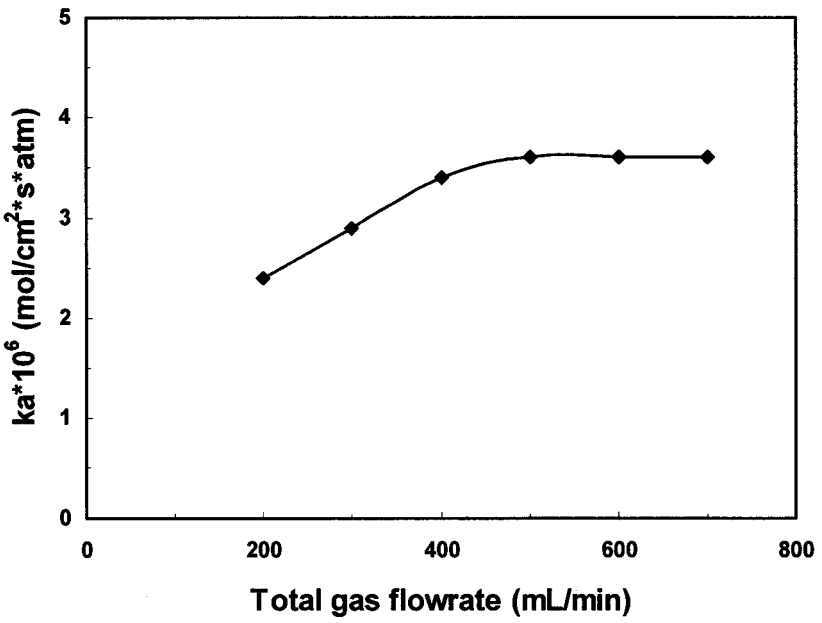

Figure 3.5–Rate constant versus total gas flow rate for $30TiO_2$-35CaO- $35SiO_2$ (wt pct) slag with CO_2/CO=1.0 and T= 1773 K.

3.4.3 Effect of Sidewall of Crucible

As discussed previously, Figure 2.10 [35] shows the comparison between calculated values of Barati's kinetic model and experimental rate constants. It can be seen that the agreement is good, but there is deviation in smaller rate constant range.

The measurement of kinetic parameters at high temperature may involve random and systematic errors, such as high gas flowrate leading to the formation of a crater and the change of oxygen potential affecting the wetting of crucible then changing the curvature of slag surface, also unwanted fluctuations in the gas flowrate included. The

sources of errors are sometimes inevitable, and all these uncertainties seem not to be the cause of the observed deviation.

When checking the experimental setup, it was found that the exposed sidewall of crucible may be the source of deviation. To test the effect of sidewall of crucible, a 12mm height platinum crucible was used, and a series experiments with slag $30FeO_x$-CaO-SiO_2 (CaO/SiO_2=1, molar ratio) was carried out. The CO_2/CO ratio was changed from 0.5 to 5.0, and different slag weights were employed to achieve the different exposed area of crucible. If there is no sidewall effect, the measured rate constants should remain the same for all crucible heights. The results are shown in Figure 3.6.

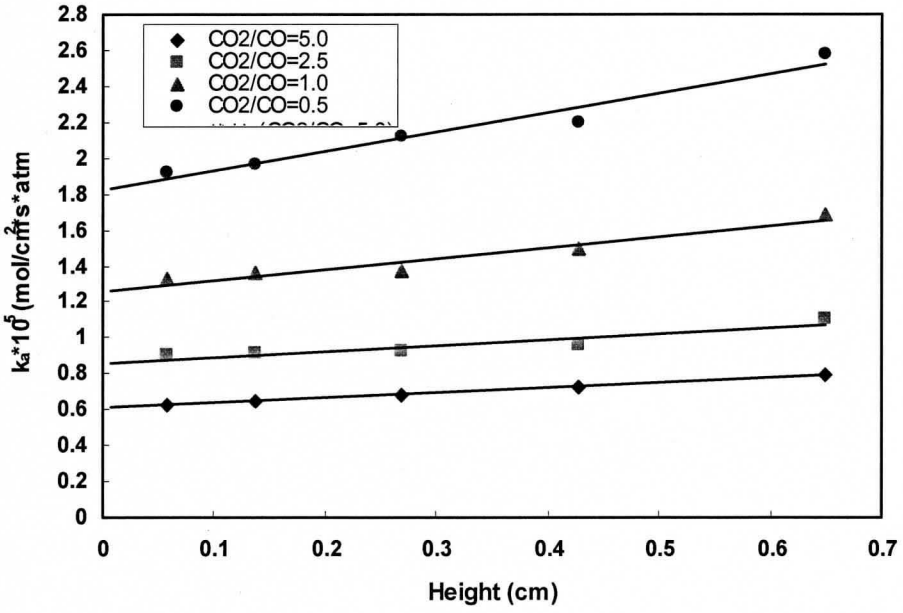

Figure 3.6–Apparent rate constant as a function of exposed height of crucible for 30FeO-CaO-SiO_2 (wt pct) slag at unit CaO/SiO_2 molar ratio.

It can be seen that the sidewall effect does exist, and the slope is a function of the rate constant for the gas/platinum reaction. When the rate constant of the gas/slag reaction is smaller, the rate on the exposed area of the platinum crucible can not be ignored, which leads to the deviation. It is difficult to control zero exposed height because of the wetting and creeping of slag, but keeping the exposed height below 2mm is possible and the error can be controlled to below 15 pct, also the measured rate constant can be adjusted to eliminate the sidewall effect by mathematical calculation. Therefore, the 8mm height platinum crucible was employed in the main experiments in the current work and the measured rate constants were all adjusted to account for the sidewall effect.

Chapter 4

EXPERIMENTAL RESULTS

In order to understand the kinetics of reaction between CO_2/CO and MnO_x/TiO_x containing slags, the dependency of the apparent rate constant (k_a) on four separate variables is studied for MnO_x/TiO_x–CaO–SiO_2 slags; oxygen potential in the gas (CO_2/CO), MnO_x/TiO_x content in the slag, slag basicity (CaO/SiO_2 ratio) and temperature. All the experimental results are given in this chapter, as is the discussion of whether the kinetic data fit with Barati's kinetic model.

4.1 Kinetics of CO_2/CO Reaction with MnO_x-CaO-SiO_2 Slags

4.1.1 Effect of Oxygen Potential

Two series of experiments were conducted at 1773K for MnO_x-CaO-SiO_2 slags. In the first series of experiments, the weight percent of Mn_2O_3 was between 10% and 40% with unit molar CaO/SiO_2 ratio; in the second series of experiments, the molar ratio of CaO/SiO_2 ratio was 0.4, 0.7, 1.2, respectively with 30% wt pct Mn_2O_3. According to the phase diagram of MnO-CaO-SiO_2, the melting points of selected range of slags are below 1773K.

The dependence of the apparent rate constant on the CO_2/CO ratio for all slag compositions are presented in logarithmic form in Figure 4.1, and results for the two series of experiments are shown in Figure 4.1(a) and Figure 4.1(b), respectively.

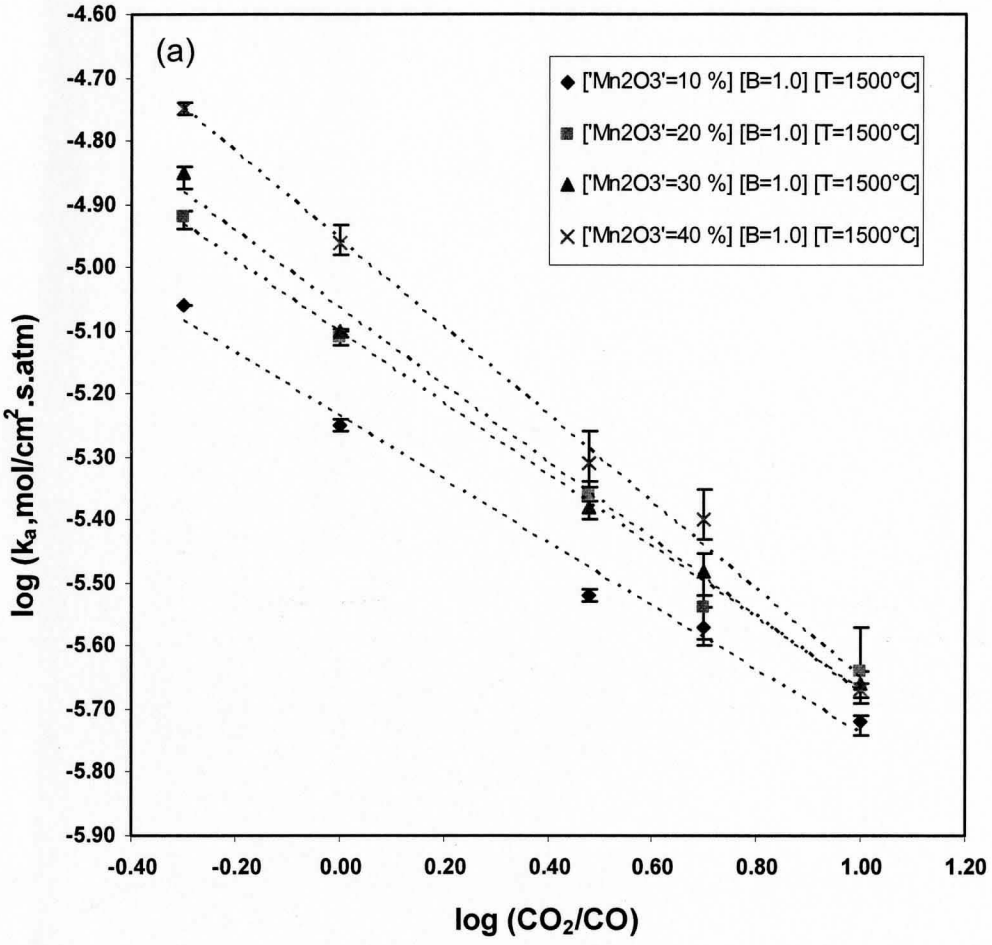

Figure 4.1 (a)

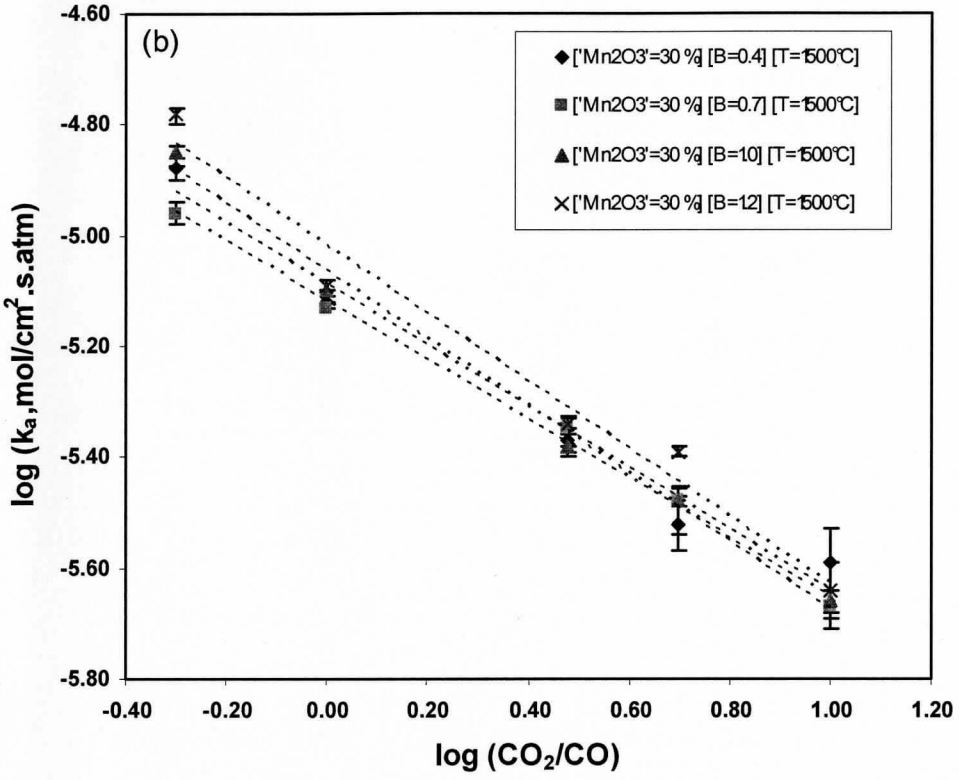

Figure 4.1-Apparent rate constant as a function of the equilibrium CO_2/CO ratio for different slags.

Figure 4.1 shows a similar linear relationship between $\log k_a$ and $\log(CO_2/CO)$ as that for FeO_x-CaO-SiO_2 slags[32,48]. The apparent rate constant can then be expressed as:

$$k_a = k_a^{\circ}(a_O)^{-\alpha} \qquad [4.1]$$

The intercepts, $\log k_a^{\,0}$, are slightly greater than that for FeO_x-CaO-SiO_2 slags, indicating that as for MO_x-CaO-SiO_2 slags at 1773K and unit molar ratio of CaO/SiO_2,

the apparent rate constant on MnO_x containing slags is greater than that on FeO_x containing slags. This is consistent with the findings of Sun[36].

The dependence of α on the manganese oxide content of the slags is shown in Figure 4.2. The values of α are between 0.5 at 10 wt pct MnO_x and 0.7 at 40 wt pct MnO_x and the empirical relationship can be expressed as

$$\alpha = 0.006 \times \%Mn_2O_3 + 0.4421 \qquad [4.2]$$

This result is consistent with that of Barati's study[32,48] and with the single charge transfer model indicating that the theoretical α does not take explicit values 0.5 or 1.0 and it may adopt intermediate values depending on the experimental conditions.[35]

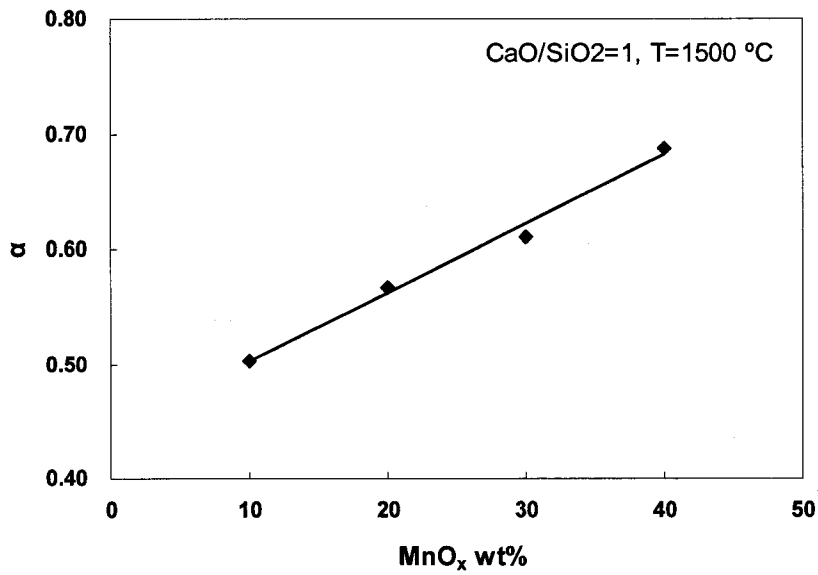

Figure 4.2-Degree of dependence of the apparent rate constant on the oxygen potential, α, as a function of manganese oxide content.

4.1.2 Effect of Manganese Oxide Content

Figure 4.3 shows the dependence of the apparent rate constant on the manganese oxide content, it can be seen that k_a increased with manganese oxide content. The trendline shows a second order polynomial relationship between k_a and manganese oxide content, which is consistent with the single charge transfer model. Barati's study[48] suggests that the content of iron oxide will affect the optical basicity and activation energy, also the Fe^{3+}/Fe^{2+} ratio is strongly dependent on the iron oxide content when CaO/SiO_2 ratio is very different from 1. This concept may also be employed for manganese oxide.

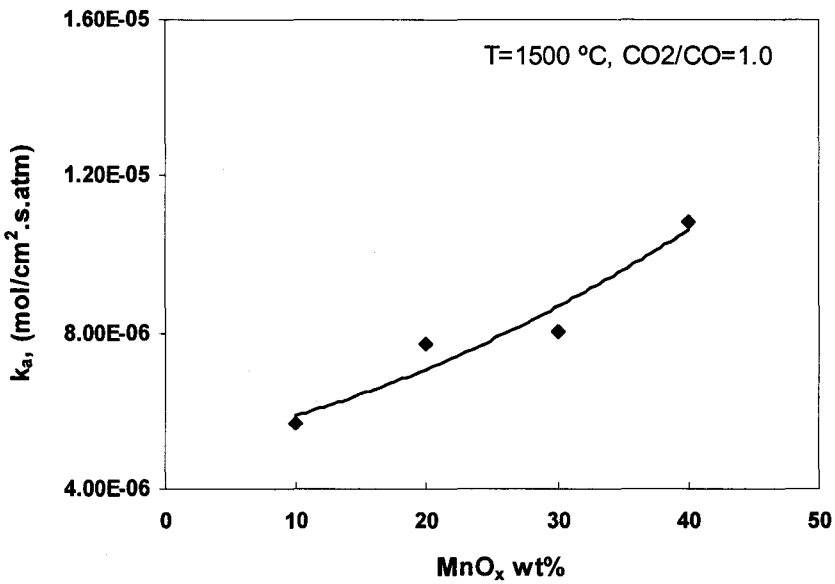

Figure 4.3-Dependence of the apparent rate constant at unit CO_2/CO and CaO/SiO_2 on the manganese oxide content at 1773K.

4.1.3 Effect of Slag Basicity

Figure 4.4 shows the dependence of the rate constant on the slag basicity. It can be seen that k_a increases with the basicity. The trend is same as that for FeO_x containing slags.

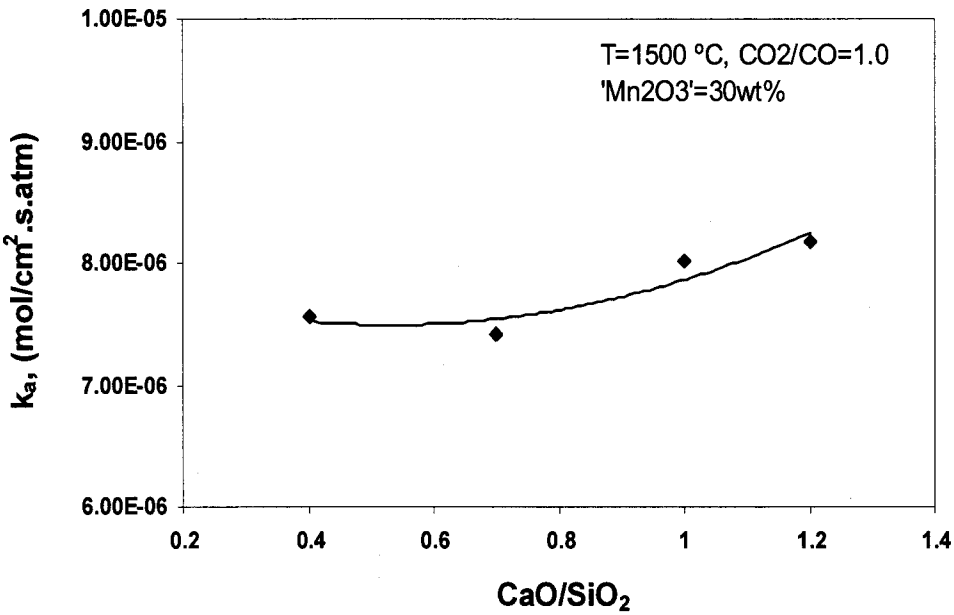

Figure 4.4-Dependence of the apparent rate constant at unit CO_2/CO on the CaO/SiO_2 at 30 wt pct MnO_x.

As reviewed previously, the effect of slag basicity on the rate constant may be discussed with regard to the effect on the redox couple ratio, Mn^{3+}/Mn^{2+}. Figure 4.5 shows the dependence of some redox ratios on slag basicity. The ratios of concentration of the oxidized ions to that of the reduced ions at a given oxygen

activity for Mn, Ti, and V all increase with slag basicity, similar to the behavior of the redox reaction of iron oxides.[36]

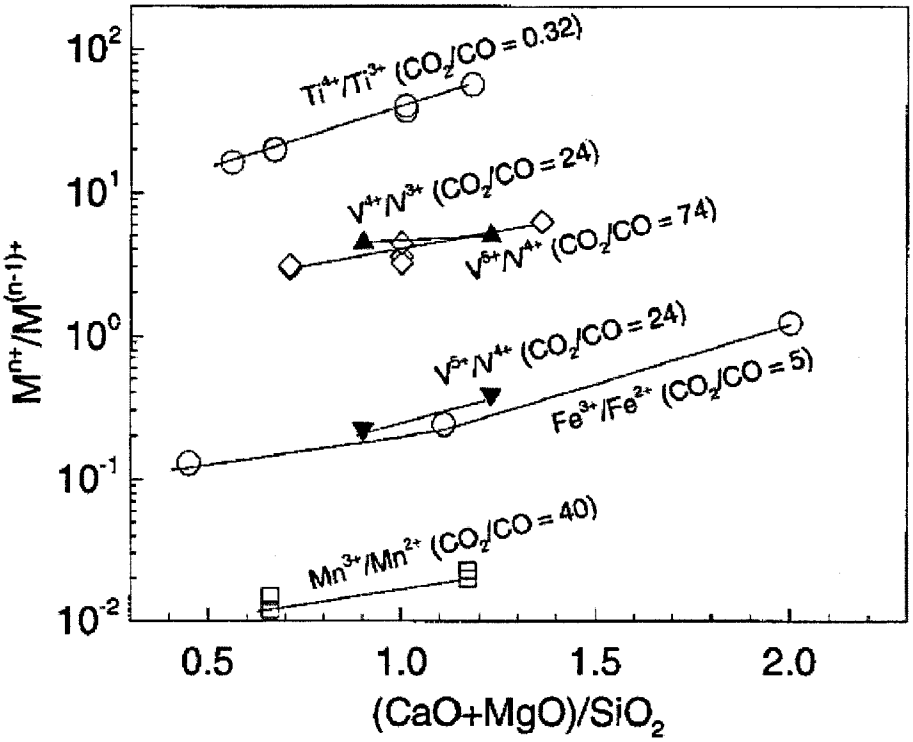

Figure 4.5-Dependence of the equilibrium redox ratio on slag basicity defined as $(CaO+MgO)/SiO_2$.[36]

Barati et al.[35] suggested a much stronger effect of slag basicity in changing the apparent activation energy. The increase in the rate constant was due to a lowering activation energy, which was caused by increasing slag basicity. Figure 4.6 shows the dependence of activation energy on optical basicity, and the result can be presented in the form:

$$E_a = 308.3 - 100.3\Lambda \quad (kJ/mol) \qquad [4.3]$$

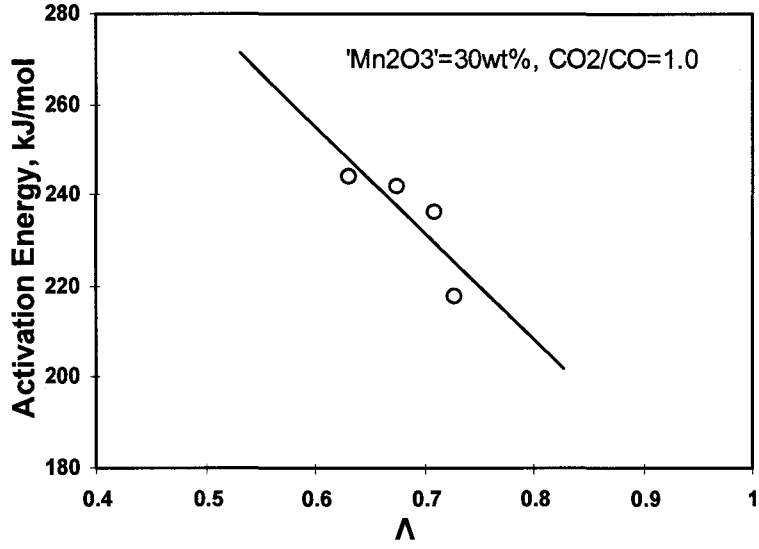

Figure 4.6-Activation energy of the reaction at unit CO_2/CO as a function of optical basicity of the slag, for melts with 30 wt pct 'Mn_2O_3'.

4.1.4 Effect of Temperature

The dependence of the apparent rate constant on temperature is expressed by the Arrhenius equation as:

$$k_a = k_a^{\,0} \exp(\frac{-E}{RT}) \qquad [4.4]$$

Where E is activation energy, R is the gas constant.

The results are shown in Figure 4.7. The slope of the Arrhenius plot, -E/R, is essentially constant for all manganese oxide contents at unit CaO/SiO_2, only the pre–exponential term, $k_a^{\ 0}$, changes with manganese oxide content.

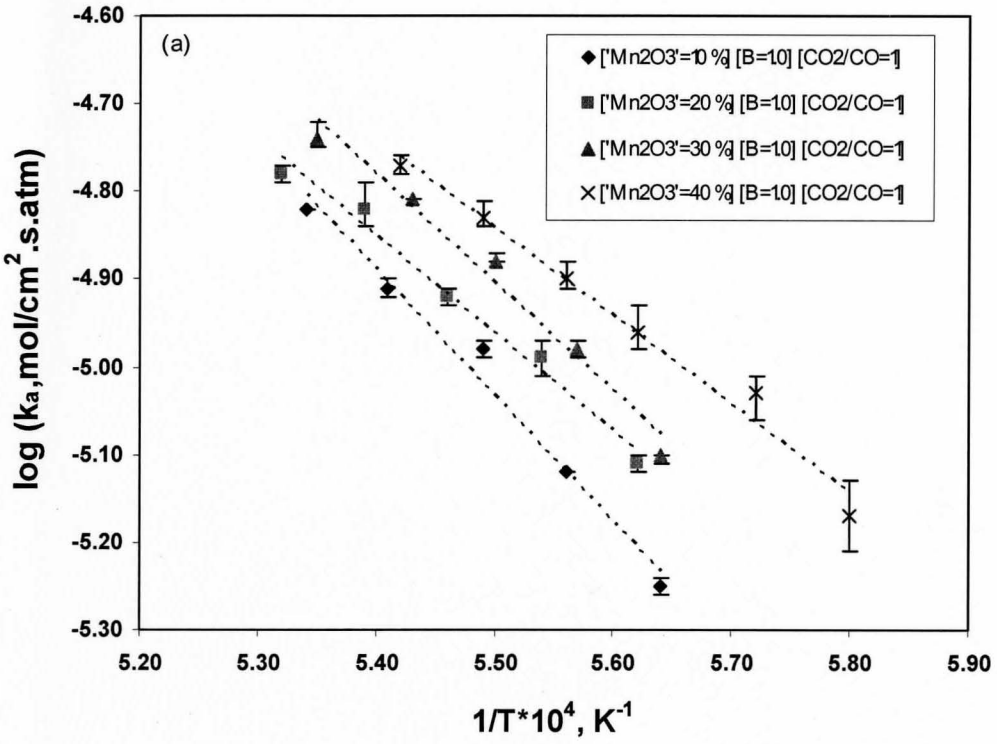

Figure 4.7 (a)

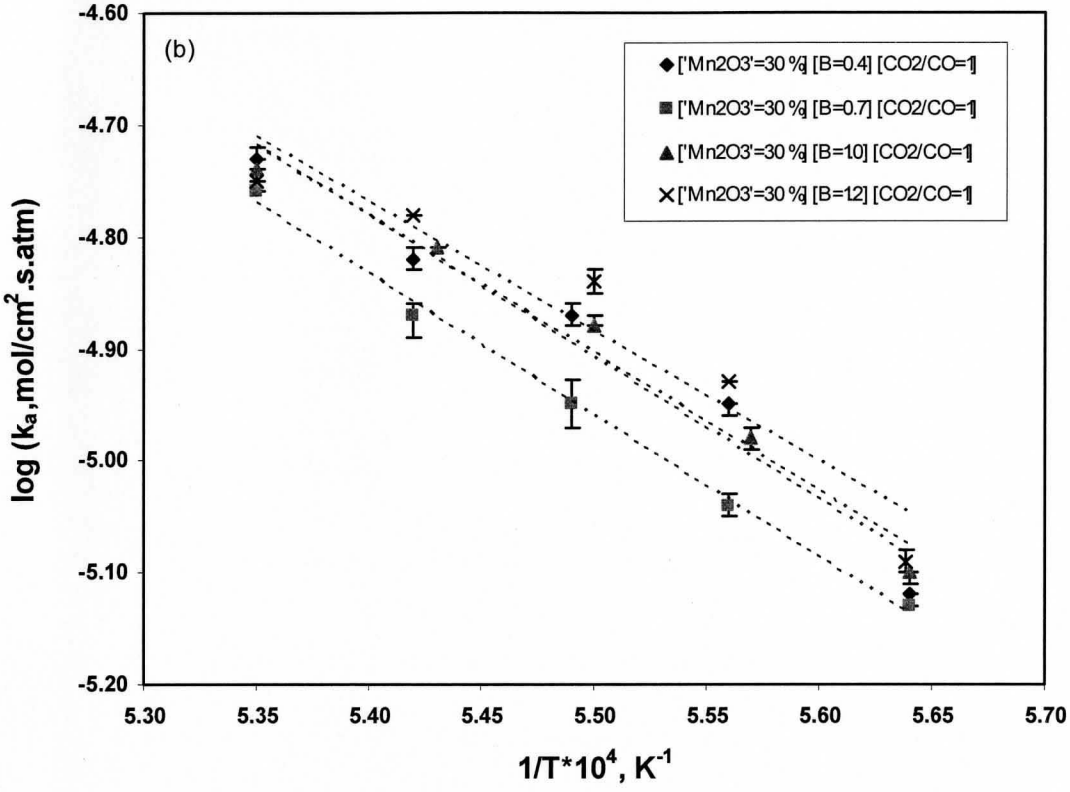

Figure 4.7-Arrhenius plot of the apparent rate constant.

Figure 4.8 shows the activation energies for slags with different manganese oxide contents. It is seen that activation energy at an average value of 228 kJ/mol is essentially independent of the manganese oxide content for slags with unit basicity.

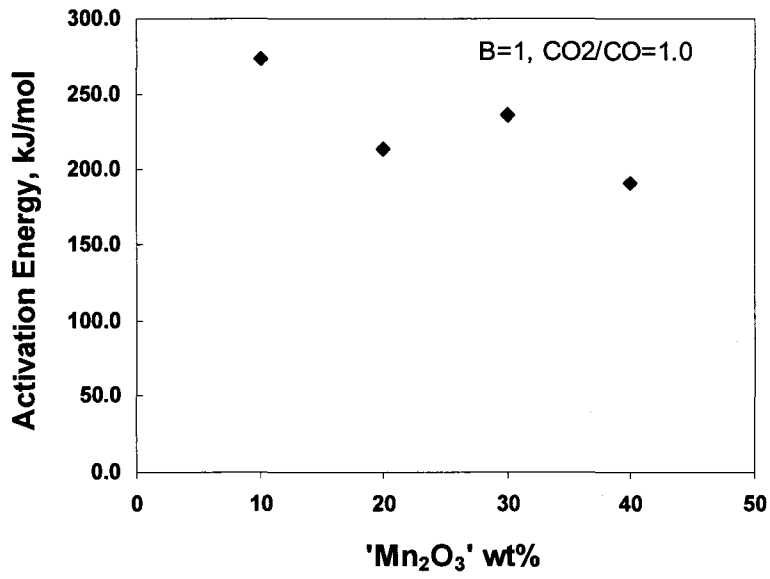

Figure 4.8-Measured activation energy at unit CO_2/CO, as a function of 'Mn_2O_3' content, for melts with CaO/SiO_2=1.0.

4.2 Kinetics of CO_2/CO Reaction with TiO_x-CaO-SiO_2 Slags

4.2.1 Effect of Oxygen Potential

Two series of experiments were conducted at 1773K for TiO_x-CaO-SiO_2 slags. In the first series of experiments, the weight percent of TiO_2 was between 10% and 50% with unit molar CaO/SiO_2 ratio; in the second series of experiments, the molar ratio of CaO/SiO_2 ratio was 0.8, 1.2, respectively with 30% wt pct TiO_2. According to the phase diagram of TiO_2-CaO-SiO_2, the melting points of selected range of slags are below 1773K.

The dependence of the apparent rate constant on the CO_2/CO ratio for all slag compositions are presented in logarithmic form in Figure 4.9, and results for the two series experiments are shown in Figure 4.9(a) and Figure 4.9(b), respectively.

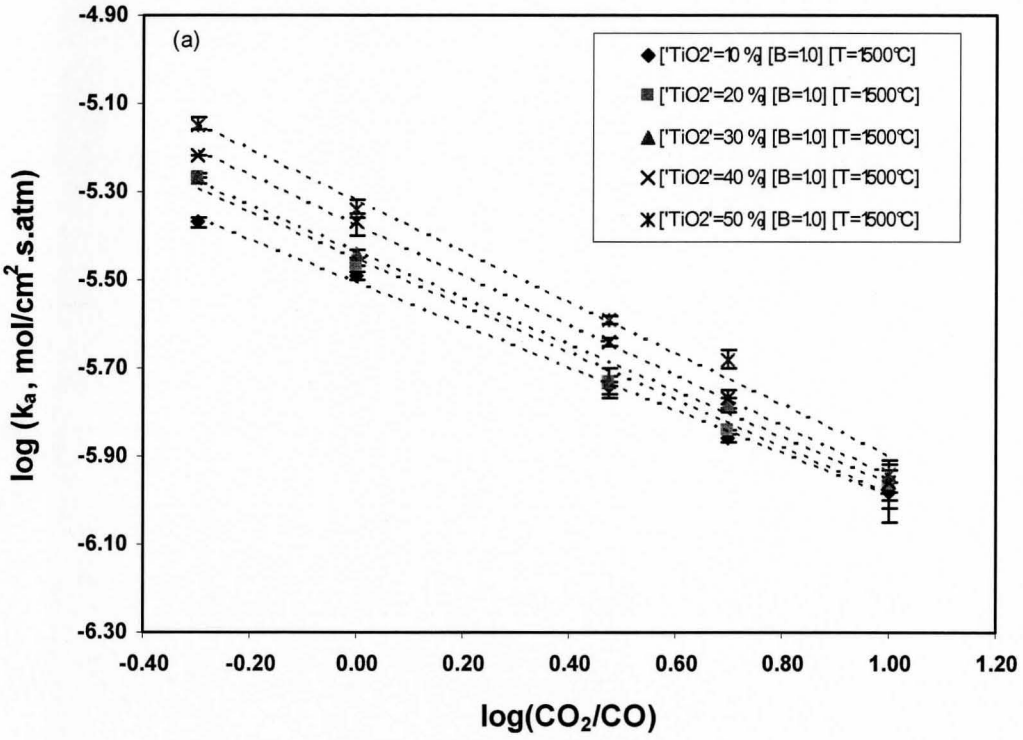

Figure 4.9(a)

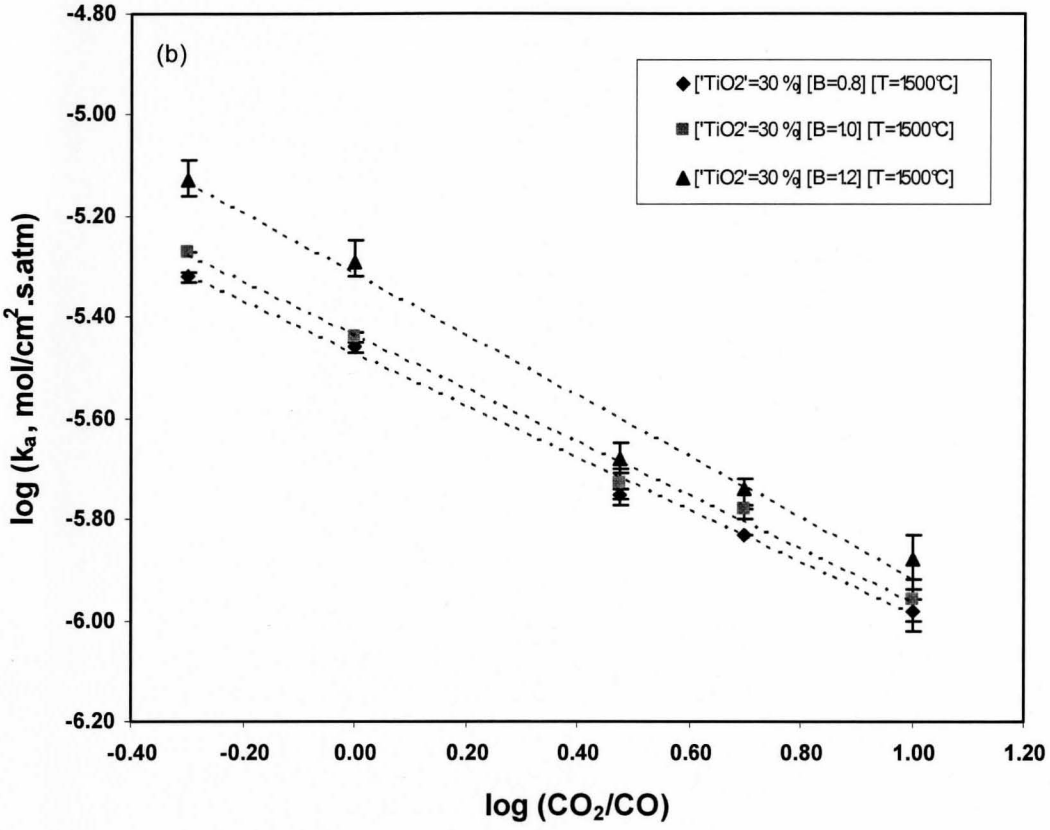

Figure 4.9-Apparent rate constant as a function of the equilibrium CO_2/CO ratio for different slags.

The apparent rate constant obtained for TiO_x containing slags shows similar behavior to that of MnO_x and FeO_x containing slags and the values of apparent rate constant are smaller than those of MnO_x and FeO_x containing slags at 1773K and unit molar ratio of CaO/SiO_2.

The dependence of α on the titanium oxide content of the slags is shown in Figure 4.10. The values of α are between 0.5 at 10 wt pct TiO_x and 0.6 at 50 wt pct TiO_x

and the empirical relationship can be expressed as

$$\alpha = 0.002 \times \%TiO_2 + 0.4729 \qquad [4.5]$$

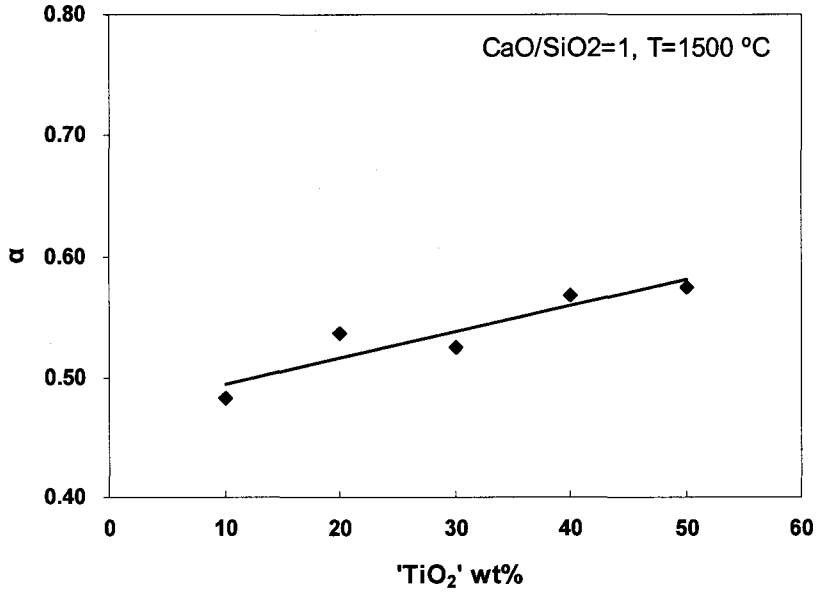

Figure 4.10-Degree of dependence of the apparent rate constant on the oxygen potential, α, as a function of titanium oxide content.

It is still consistent with that of Barati's study[35] and values of α take intermediate values between 0.5 and 1 depending on the experimental conditions although the effect of TiO_x is not as strong as that of FeO_x and MnO_x.

4.2.2 Effect of Titanium Oxide Content

Figure 4.11 shows the dependence of the apparent rate constant on the titanium oxide content, it can be seen that k_a increased with titanium oxide content. The trendline also shows a second order polynomial relationship between k_a and titanium oxide content, which is consistent with the single charge transfer model and follows similar behavior to that of MnO_x and FeO_x containing slags. The values of apparent rate constant for TiO_x containing slags are also smaller than those of FeO_x and MnO_x containing slags at same weight percent of MO_x and same other experimental conditions.

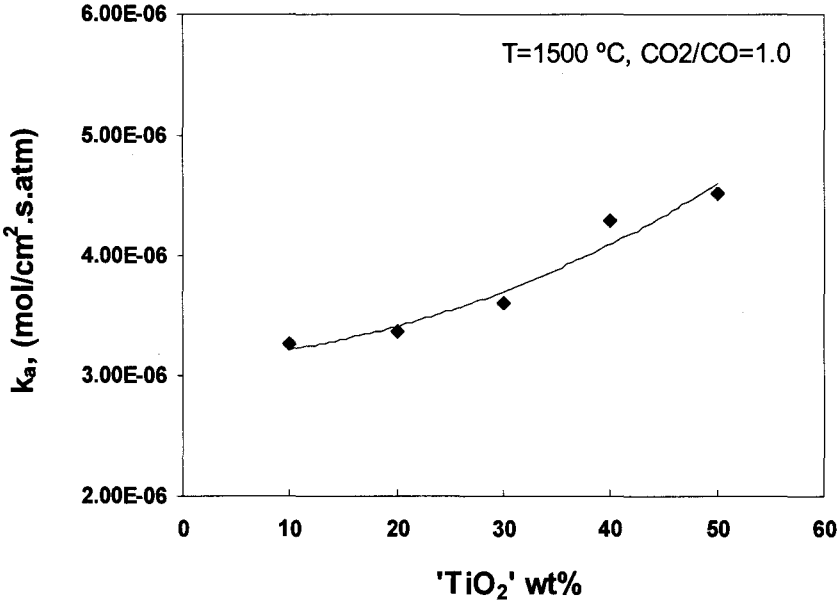

Figure 4.11-Dependence of the apparent rate constant at unit CO_2/CO and CaO/SiO_2 on the titanium oxide content at 1773K.

4.2.3 Effect of Slag Basicity

Figure 4.12 shows the dependence of the rate constant on the slag basicity. It can be seen that k_a increases with the basicity. The trend is same as that for FeO_x and MnO_x containing slags.

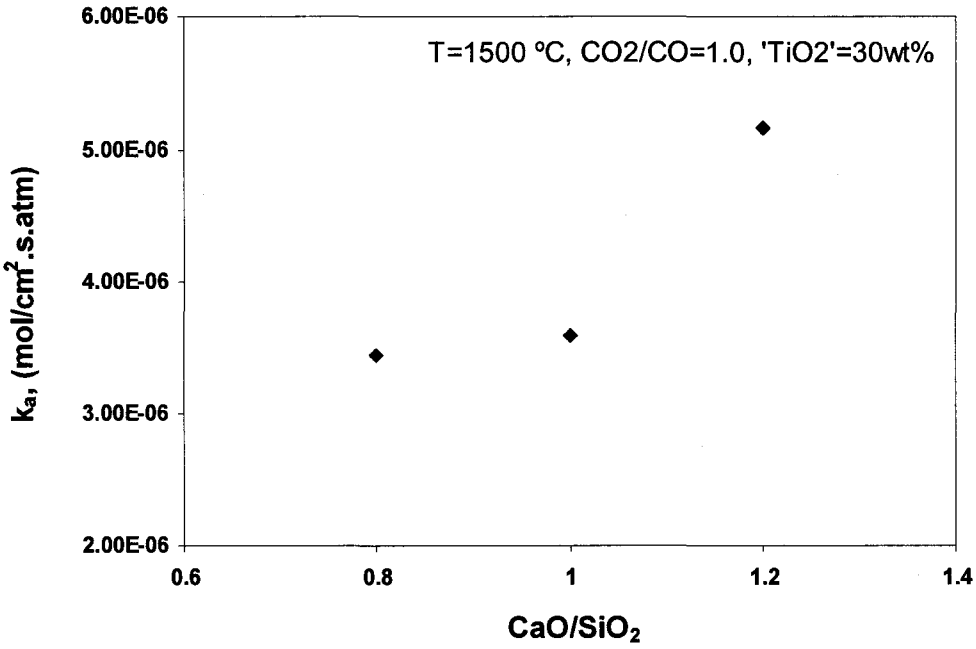

Figure 4.12-Dependence of the apparent rate constant at unit CO_2/CO on the CaO/SiO_2 at 30 wt pct 'TiO_2'.

As discussed previously, changing the bulk composition of the slag would influence the rate constant by two factors. One effect of basicity is in changing the apparent activation energy of the reaction, increasing the slag basicity will decrease the

activation energy, thereby increasing the rate constant. Figure 4.13 shows the dependence of activation energy on optical basicity, and the result can be presented in the form:

$$E_a = 846.6 - 834.1\Lambda \quad (kJ/mol) \qquad [4.6]$$

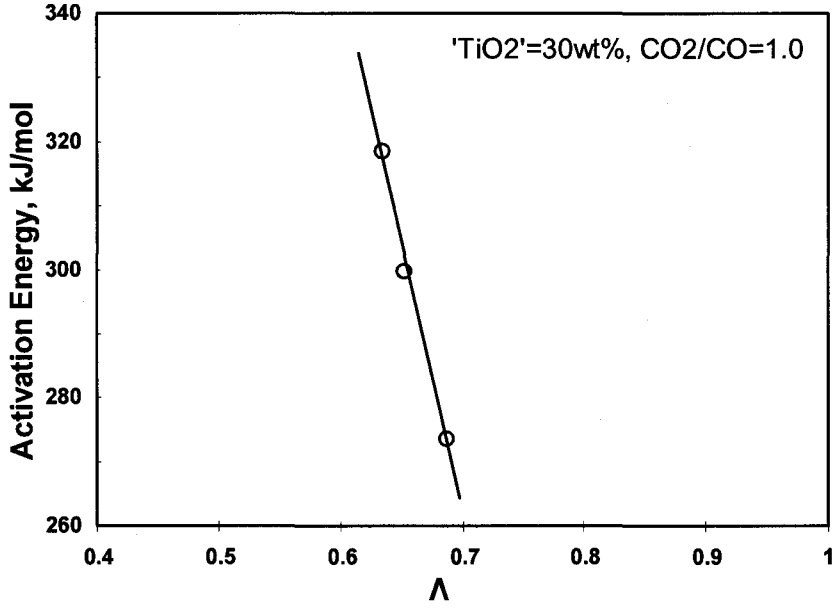

Figure 4.13-Activation energy of the reaction at unit CO_2/CO as a function of optical basicity of the slag, for melts with 30 wt pct 'TiO_2'.

Another effect of slag basicity on the rate constant may be via the effect on the redox couple ratio, Ti^{4+}/Ti^{3+} increases with the slag basicity at a given oxygen activity, similar to the behavior of redox reaction of iron oxides and manganese oxides.[36] Trannel et al.[67] found that increasing TiO_x content from 7 to 14 wt pct increased the Ti^{4+}/Ti^{3+} ratio at a given temperature and oxygen activity, and further addition of TiO_x did not follow the same trend. This observation was attributed to the possibility of formation of complex anions in high titania slags.

It can be seen from Figure 4.5 that at a given oxygen activity and slag basicity, the redox ratio in MO_x-CaO-SiO_2 slags appears to be $Ti^{4+}/Ti^{3+} > Fe^{3+}/Fe^{2+} > Mn^{3+}/Mn^{2+}$, as greater concentration of the more reduced species leads to higher free electron concentration, this may explain the gradual increase of the value of apparent rate constant for TiO_x, FeO_x and MnO_x containing slags at same experimental conditions.

4.2.4 Effect of Temperature

Figure 4.14 shows the Arrhenius plot of the apparent rate constant measured at unit CO_2/CO ratio for all TiO_x slag samples. The slope of the Arrhenius plot is essentially constant for all titanium oxide contents at unit CaO/SiO_2, only the pre–exponential term changes with titanium oxide content.

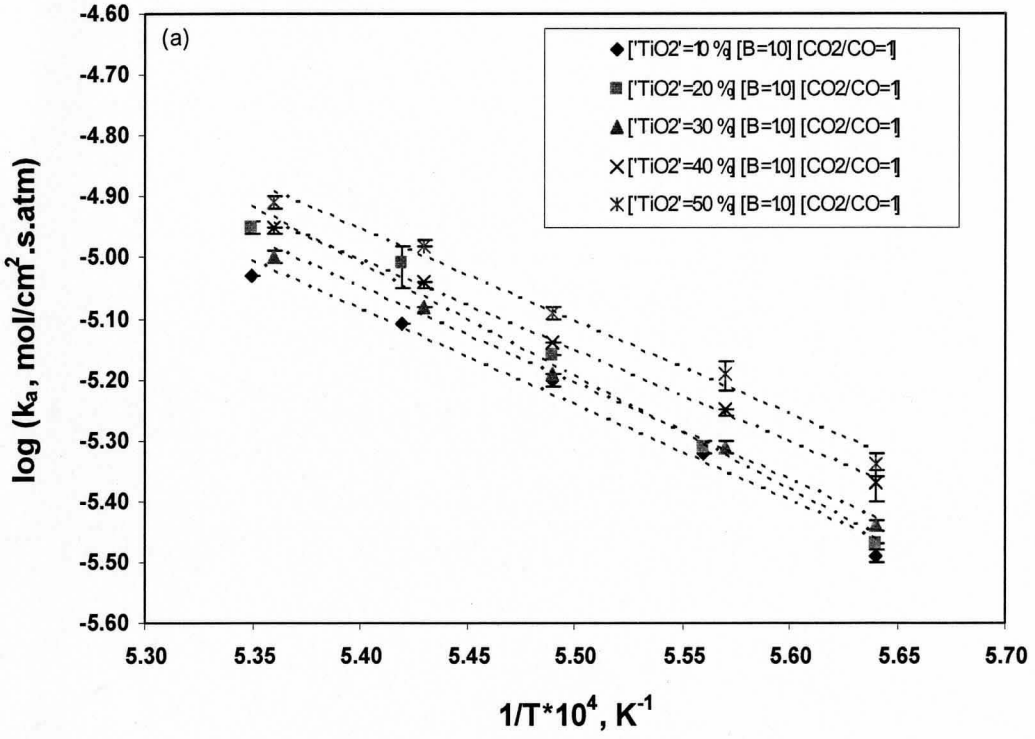

Figure 4.14(a)

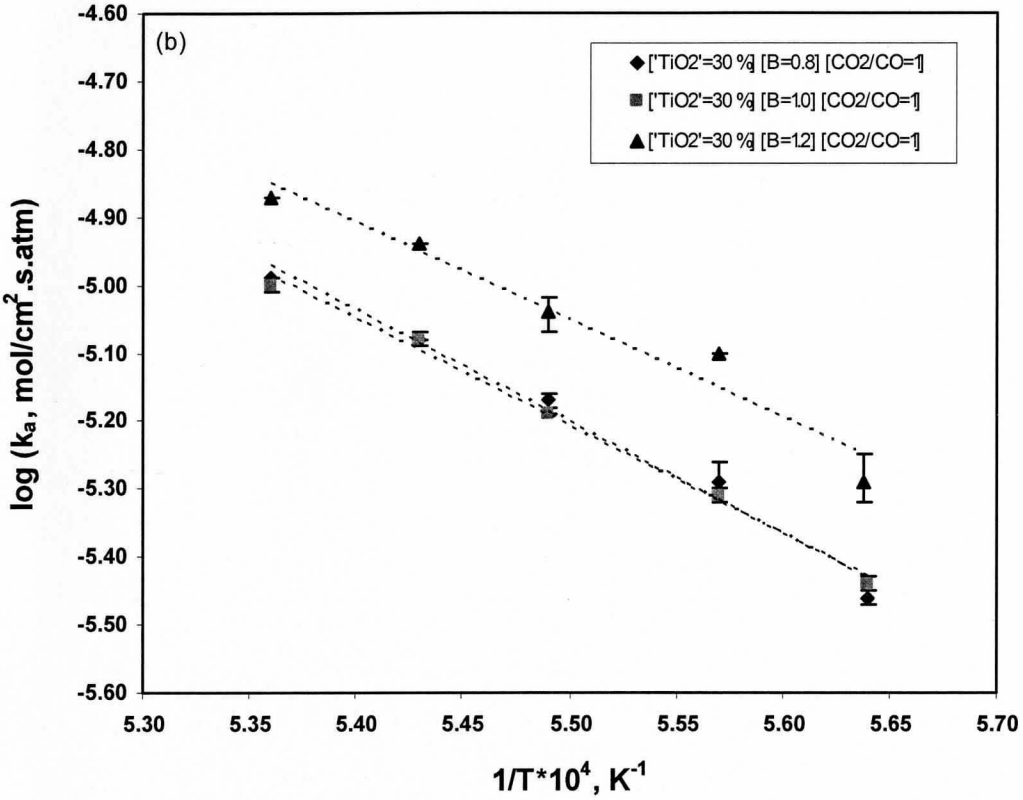

Figure 4.14-Arrhenius plot of the apparent rate constant.

Figure 4.15 shows the activation energies for slags with different titanium oxide contents. It is seen that activation energy at an average value of 309 kJ/mol is essentially independent of the titanium oxide content for slags with unit basicity, which is greater than 228 kJ/mol for the reaction with manganese oxides.

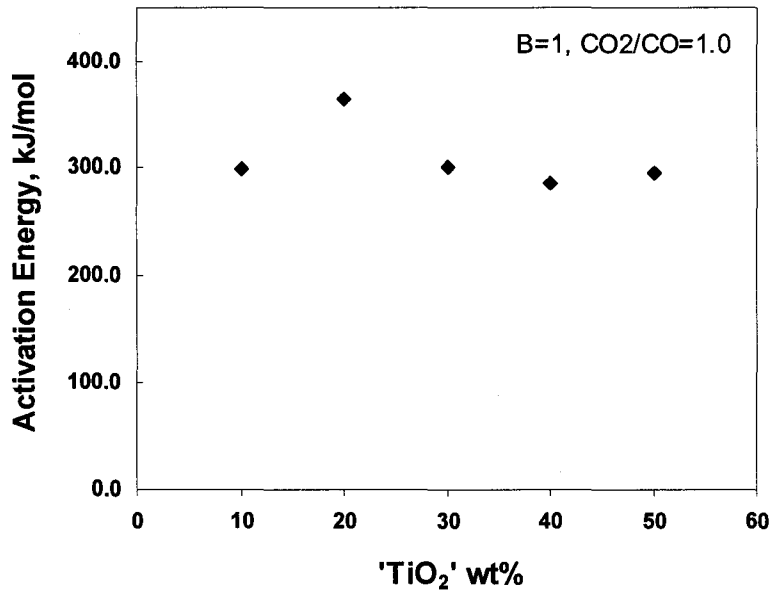

Figure 4.15-Measured activation energy at unit CO_2/CO, as a function of 'TiO_2' content, for melts with CaO/SiO_2=1.0.

4.3 Validation of the Single Charge Transfer Model

As reviewed previously, in single charge transfer model, the form of the rate constant expression is presented as

$$k_a = k^{\circ}\left(C_M\right)^2 \frac{1}{r(1+r)^2}\exp\left(\frac{-E_a}{RT}\right) \qquad [4.7]$$

where in this equation,

k° : global constant for the reaction;

C_M : total metal concentration in the bulk in molar percent;

r : ratio of $M^{(n+1)+}/M^{n+}$;

E_a : apparent activation energy.

There are not sufficient data for redox equilibria, Mn^{3+}/Mn^{2+} and Ti^{4+}/Ti^{3+}, for different slags reported, some data from the study by Sun et al.[36] and Tranell et al.[68] are used in the calculation, and the empirical correlation derived by Yang and Belton[57] is employed to calculate the other redox equilibria data.

The correlation between the optical basicity and apparent activation energy is shown in Equation [4.3] and [4.6] for MnO_x and TiO_x containing slags, respectively. To calculate the optical basicity, $\Lambda_{SiO_2} = 0.48$, $\Lambda_{CaO} = 1.0$, $\Lambda_{MnO} = 0.95$ and $\Lambda_{TiO_2} = 0.65$ were used.[69]

4.3.1 Model for Manganese Oxide Containing Slags

To determine the global value of k°, the rate constants measured at unit CO_2/CO ratio, unit CaO/SiO_2 molar ratio and 1773K within the range of manganese oxide between 10% to 40% were used. The result is shown in Figure 4.16, in which the trendline yield

$$k^\circ = 1.1\times10^{-6} \quad (mol.cm^{-2}.atm^{-1}.s^{-1}) \qquad [4.8]$$

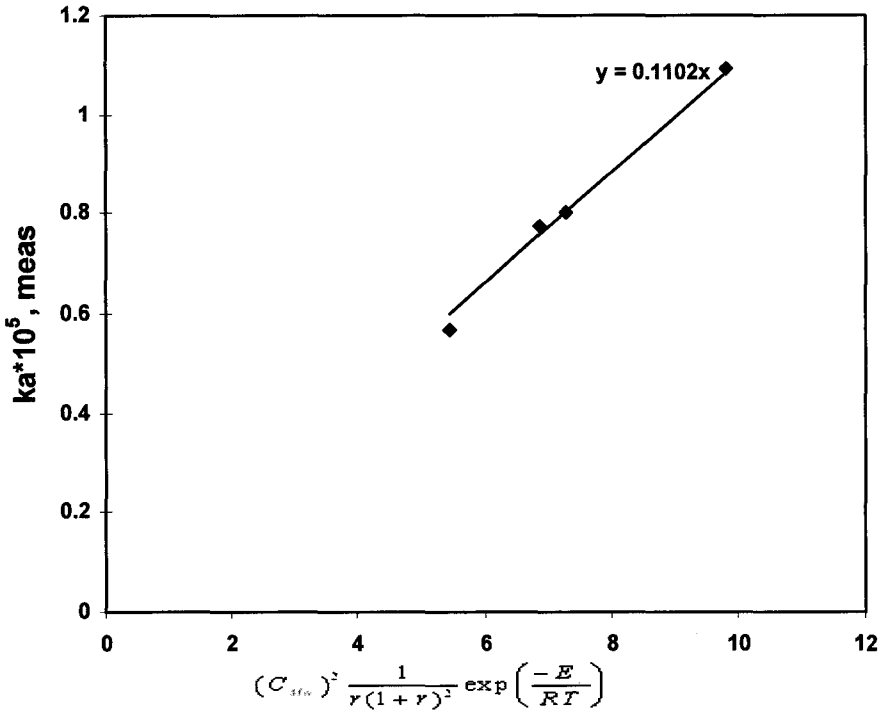

Figure 4.16-The measured rate constant as a function of $(C_{Mn})^2 \frac{1}{r(1+r)^2}\exp\left(\frac{-E_a}{RT}\right)$

(derivation of k°**).**

The final form of rate constant expression for manganese oxide containing slags is given by

$$k_a = 1.1\times10^{-6}\times(C_{Mn})^2 \frac{1}{r(1+r)^2}\exp\left(\frac{-(308.3-100.3\Lambda)}{RT}\right) \quad (mol.cm^{-2}.atm^{-1}.s^{-1}) \qquad [4.9]$$

Figure 4.17 shows the results of the experimental rate constants in comparison with the calculated values for manganese oxide containing slags. Considering the extent of error involved in the experiments, the agreement is good. Because of the elimination

of sidewall effect of the crucible, there is no deviation at the range of smaller rate constants.

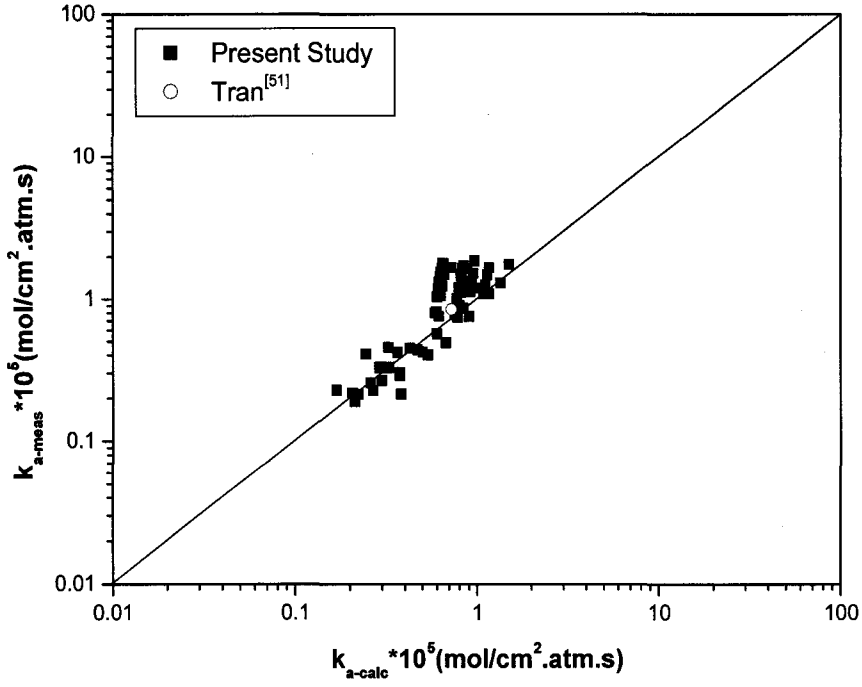

Figure 4.17-Comparison between the calculated and the measured rate constant under various experimental conditions.

As for the calculated values of redox equilibria ratio, the difference is very small when only changing the temperature and keeping the other experimental conditions unchanged, the calculated rate constants are nearly same. Therefore it looks like four groups of vertical points in Figure 4.17. More accurate data for redox equilibria ratio may solve the problem. Figure 4.18 shows the comparison results with the

experimental conditions from only one temperature. The agreement is better than that in Figure 4.17.

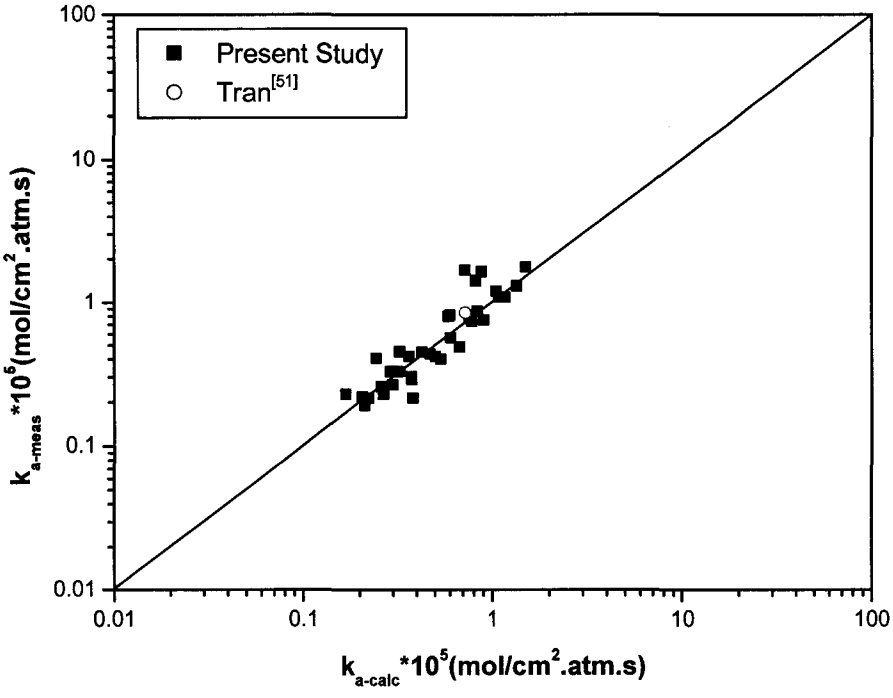

Figure 4.18-Comparison between the calculated and the measured rate constant under various experimental conditions(T=1773K).

4.3.2 Model for Titanium Oxide Containing Slags

To determine the global value of k°, the rate constants measured at unit CO_2/CO ratio, unit CaO/SiO_2 molar ratio and 1773K within the range of titanium oxide between 10% to 50% were used. The result is shown in Figure 4.19, in which the trendline yield

$$k^{\circ} = 4.37 \times 10^{-4} (mol.cm^{-2}.atm^{-1}.s^{-1}) \qquad [4.10]$$

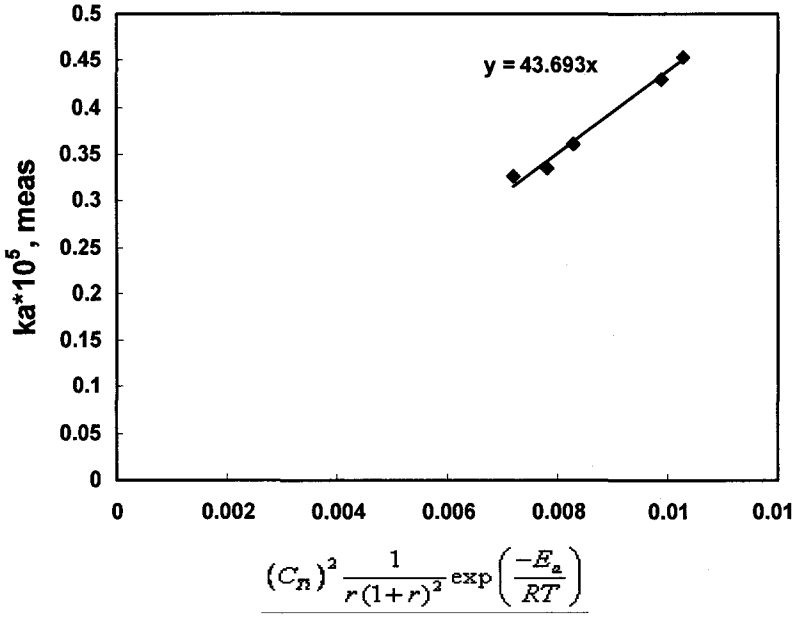

Figure 4.19-The measured rate constant as a function of $(C_{Ti})^2 \frac{1}{r(1+r)^2} \exp\left(\frac{-E_a}{RT}\right)$ **(derivation of** k°**).**

The final form of rate constant expression for titanium oxide containing slags is given by

$$k_a = 4.37\times10^{-4}\times(C_{Ti})^2\frac{1}{r(1+r)^2}\exp\left(\frac{-(846.6-834.1\Lambda)}{RT}\right)\quad (mol.cm^{-2}.atm^{-1}.s^{-1}) \qquad [4.11]$$

Figure 4.20 shows the results of the experimental rate constants in comparison with the calculated values for titanium oxide containing slags. There is a good fit between the two values and the rate expression can be applied to calculate the rate constant.

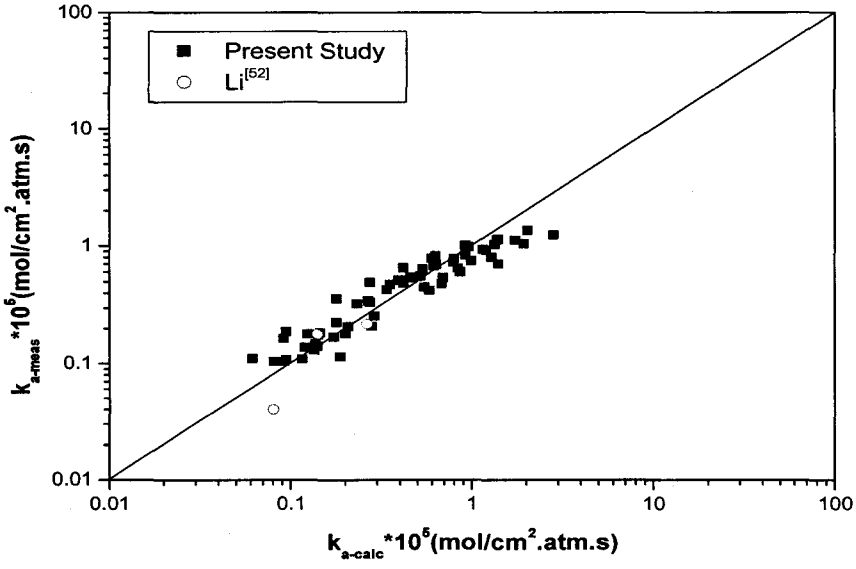

Figure 4.20-Comparison between the calculated and the measured rate constant under various experimental conditions.

Chapter 5

CONCLUSIONS

The apparent rate constant of interfacial reaction between CO_2/CO and molten MnO_x/TiO_x-CaO-SiO_2 slags were measured using ^{13}C isotope exchange method. A broad range of experimental conditions including oxygen potential, manganese and titanium oxide content, slag basicity and temperature were examined in the experiments.

5.1 Conclusions

1. The apparent rate constant for dissociation of CO_2 on the surface of MnO_x/TiO_x -CaO-SiO_2 slags decreases with increasing the equilibrium oxygen potential, according to:

$$k_a = k_a^{\circ}(a_O)^{-\alpha}$$

The parameter α is dependent on slag composition. At unit CaO/SiO_2, the empirical relationship can be expressed as

$$\alpha = 0.006 \times \%Mn_2O_3 + 0.4421$$

for manganese oxide containing slags and

$$\alpha = 0.002 \times \%TiO_2 + 0.4729$$

for titanium oxide containing slags.

2. The apparent rate constant increases with MnO_x/TiO_x content of the slags.

3. The apparent rate constant increases with increasing the slag basicity by decreasing the apparent activation energy. The dependence of activation energy on optical basicity can be expressed as

$$E_a = 308.3 - 100.3\Lambda \quad (kJ/mol)$$

For manganese oxide containing slags and

$$E_a = 846.6 - 834.1\Lambda \quad (kJ/mol)$$

For titanium oxide containing slags.

4. The apparent rate constant follows an Arrhenious relationship with temperature. The measured activation energy of the reaction was independent of manganese or titanium oxide content at unit CaO/SiO_2. The average values of activation energy are 228 kJ/mol and 309 kJ/mol for interfacial reaction between CO_2/CO and manganese oxide and titanium oxide containing slags, respectively.

5. The apparent rate constants gradually increase for TiO_x, FeO_x and MnO_x containing slags at same experimental conditions, which may be caused by that at a given oxygen activity and slag basicity, the redox ratio in MO_x-CaO-SiO_2 slags appears to be

$Ti^{4+}/Ti^{3+}>Fe^{3+}/Fe^{2+}>Mn^{3+}/Mn^{2+}$.

6. The apparent rate constants measured for MnO_x and TiO_x containing slags show similar behavior to that of FeO_x containing slags and the kinetic data can be fitted well in the single charge transfer model proposed by Barati and Coley. The rate constant expression for manganese oxide containing slags is given by

$$k_a = 1.1\times10^{-6}\times(C_{Mn})^2\frac{1}{r(1+r)^2}\exp\left(\frac{-(308.3-100.3\Lambda)}{RT}\right) \quad (mol.cm^{-2}.atm^{-1}.s^{-1})$$

And that for titanium oxide containing slags is given by

$$k_a = 4.37\times10^{-4}\times(C_{Ti})^2\frac{1}{r(1+r)^2}\exp\left(\frac{-(846.6-834.1\Lambda)}{RT}\right) \quad (mol.cm^{-2}.atm^{-1}.s^{-1})$$

5.2 Future Work

Because there is not sufficient data of redox equilibria for MnO_x and TiO_x containing slags, most of them are calculated by empirical correlation but not measured, which may create some deviation. To optimize the rate constant expression, accurate measurements of the redox equilibria are needed.

For gas/slag interfacial reactions, H_2 is another important reducing gas, the rate constant of reaction between H_2O/H_2 and transition metal oxide containing slags can be measured to compare with that of CO_2/CO reaction.

BIBLIOGRAPHY

1. H.H. Rodriguez, A.N. Conejo, and R.D. Morales: Steel Res., 2001, vol. 72, pp. 298-303.
2. M. Ozawa, S. Kitagawa, S. Nakayama, and Y. Takesono: Trans. Iron Steel Inst. Jpn., 1986, vol. 26, pp. 621-628.
3. M. Mltagh: Iron and Steelmaker, 1991, vol. 18 (10), pp. 56-57.
4. R. Campos and L. Torres: Proc. Paul E. Qeneau Int. Symp. On Extractive Metallurgy of Copper, Nickel and Cobalt, vol. II, Copper and Mickel Smelter Operation, C. A., Landolt, ed., TMS, Warrendale, PA, 1993, pp. 1441-1460.
5. J.O. Achurra, C.H. Queirolo, and J.G. Achurra: in Copper 87, vol. 4, Pyrometallurgy of Copper, C. Diaz, C. Landolt, and A. Luraschi, eds., University of Chile, Santiago, Chile, 1987, p. 393.
6. M.W. Davies, G.S.F. Hazeldean, and P.N. Smith: Physical Chemistry of Process Metallurgy, The Richardson Conf., The Institute of Mining and Metallurgy, London, 1973, pp. 95-107.
7. T. Gore and G.S.F. Hazeldean: Ironmaking and Steelmaking, 1981, vol. 8, pp. 169-181.
8. E.W. Mulholland, G.S.F. Hazeldean, and M.W. Davies: J. Iron Steel Inst., 1973, vol. 211, pp. 632-639.
9. S. Hara and K. Ogino: Testu-to-Hagane, 1990, vol. 76, pp. 360-367.
10. G.G. Krishna Murthy, A. Hasham, and U.D. Pal: Ironmaking and Steelmaking, 1993, vol. 20, pp. 191-200.
11. D.J. Min and R.J. Fruehan: Metall. Trans. B, 1992, vol. 23B, pp. 29-37.
12. B. Sarma, A.W. Cramb, and R.J. Fruehan: Metall. Mater. Trans. B, 1996, vol. 27B, pp. 717-731.
13. N. Siddiqi, B. Bhoi, R.K. Paramguru, V. Sahajwalla, and O. Ostrovski: Ironmaking and Steelmaking, 2000, vol. 27. pp. 367-372.
14. R.J. Fruehan: Metall. Mater. Trans. B, 1997, vol. 28B, pp. 743-753.
15. D.J. Min, J.W. Han, and W.S. Chung: Metall. Mater. Trans. B, 1999, vol. 30B, pp. 215-221.
16. R.D. Morales, R. Lule, F. Lopez, J. Camacho, and J.A. Romero: Iron Steel Inst. Jpn. Int., 1995, vol. 35, pp. 1054-1062.
17. M. Sheikhshab Bafghi, H. Kurimoto, and M. Sano: Iron Steel Inst. Jpn. Int., 1992, vol. 32, pp. 1084-1090.
18. M.P. Shalimov, V.N. Boroneshkov, and S.A. Lyamkin: Russ. Metall., 1980, vol. 3, pp. 31-34.
19. F. Ji, M. Barati, K. Coley, and G.A. Irons: Proc. VII Int. Conf. on Molten Slags, Fluxes and Salts, Cape Town, SA, Jan. 25-28, 2004, pp. 399-407.
20. R.K. Paramguru, R.K. Galgali, and H.S. Ray: Metall. Mater. Trans. B, 1997, vol. 28B, pp. 805-810.
21. F. Fun: Metall. Trans., 1970, vol. 1, pp. 2537-2541.
22. G.S. Ershov and E.A. Popova: Chem. Abstr., 1964, vol. 60, p. 4166d.

23. A.K. Jouhari, R.K. Galgali, P. Chattopadhyay, R.C. Gupta, and H.S. Ray: Scand. J. Metall., 2001, vol. 30, pp. 14-20.
24. M. Sheikhshab Bafghi, Y. Ito, S. Yamada, and M. Sano: Iron Steel Inst. Jpn. Int., 1992, vol. 32, pp. 1084-1090.
25. S.R. Story, B. Sarma, R.J. Fruehan, A.W. Cramb, and G.R. Belton: Metall. Mater. Trans. B, 1998, vol. 29B, pp. 929-932.
26. D.R. Sain and G.R. Belton: Metall. Mater. Trans. B, 1976, vol. 7B, pp. 235-244.
27. D.R. Sain and G.R. Belton: Metall. Mater. Trans. B, 1978, vol. 9B, pp. 403-407.
28. F.J. Mannion and R.J. Fruehan: Metall. Mater. Trans. B, 1989, vol. 20B, pp. 853-861.
29. T. Nagasaka and R.J. Fruehan: Metall. Mater. Trans. B, 1994, vol. 25B, pp. 245-253.
30. S.R. Story and R.J. Fruehan: Metall. Mater. Trans. B, 2000, vol. 31B. pp. 43-54.
31. S.R. Story, B. Sarma, R.J. Fruehan, A.W. Cramb, and G.R. Belton: Metall. Mater. Trans. B, 1998, vol. 29B, pp. 935-938.
32. M. Barati and K. Coley: Metall. Mater. Trans. B, 2005, vol. 36B, pp. 169-178.
33. M. Barati and K. Coley: Metall. Mater. Trans. B, 2006, vol. 37B, pp. 41-49.
34. M. Barati and K. Coley: Metall. Mater. Trans. B, 2006, vol. 37B, pp. 51-59.
35. M. Barati and K. Coley: Metall. Mater. Trans. B, 2006, vol. 37B, pp. 61-69.
36. S. Sun and S. Jahanshahi: Metall. Mater. Trans. B, 2000, vol. 31B, pp. 937-943.
37. G.R. Belton: 2nd Int. Symp. on Metallurgical Slags and Fluxes, H.A. Fine and D.R. Gaskell, eds., TMS–AIME, Warrendale, PA, 1984, pp. 63–85.
38. G.R. Belton: Proc. 3rd Int. Conf. on Molten Slags and Fluxes, The Institute of Metals, London, 1989, pp. 96–106.
39. G.R. Belton: 4th Int. Conf. on Molten Slags and Fluxes, Iron and Steel Institue of Japan, Tokyo, Japan, 1992, pp. 516–524.
40. G.R. Belton and R.J. Fruehan: Turkdogan Symp. Proc., Pittsburgh, PA, ISS of AIME, 1994, pp. 3–22.
41. S.K. EL-Rahaiby, Y. Sasaki, D.R. Gaskell, and G.R. Belton: Metall. Mater. Trans. B, 1986, vol. 17B, pp. 307-316.
42. Y. Sasaki., S. Hara, D.R. Gaskell, and G.R. Belton: Metall. Mater. Trans. B, 1984, vol. 15B, pp. 563-571.
43. S. Sun and G.R. Belton: Metall. Mater. Trans. B, 1998, vol. 29B, pp. 137-145.
44. S. Sun, Y. Sasaki, and G.R. Belton: Metall. Mater. Trans. B, 1998, vol. 29B, pp. 959-965.
45. Y. Li, I.P. Ratchev, J.A. Lucas, G.M. Evans, and G.R. Belton: Metall. Mater. Trans. B, 2000, vol. 31B, pp. 1049-1057.
46. S. Sun: Ph.D. Thesis, University of Newcastle, Newcastle, Australia, 1988.
47. M. Mori, K. Morita, and N. Sano: Iron Steel Inst. Jpn. Int., 1996, vol. 36, pp. 624-630.
48. M. Barati, Ph.D. Thesis, Mcmaster University, Hamilton, ON, Canada, 2005.
49. T. Tran, S. Sun, and S. Jahanshahi: Proc. V Int. Conf. Molten Slags, Fluxes and Salts Conf., Sydney, Australia, 1997, pp. 115-123.

50. E.T. Turkdogan: Fundamental of Steelmaking, the University Press, Cambridge, UK, 1996.
51. J.A. Duffy and M.D. Ingram: Establishment of an Optical Scale For Lewis Basicity in Inorganic Oxyacids, Molten Salts, and Glasses, Journal of American Chemical Society, 1971, vol. 93, pp. 6448–6454.
52. Y. Li, and I.P. Ratchev: Metall. Mater. Trans. B, 2002, vol. 33B, pp. 651-660.
53. T. Tran, Ph.D. Thesis, University of Melbourne, Melbourne, Australia, 1997.
54. Y. Li: Ph.D. Thesis, University of Newcastle, Newcastle, Australia, 1999.
55. A.W. Cramb and G.R. Belton: Metall. Mater. Trans. B, 1981, vol. 12B, pp. 699–704.
56. C. Wagner: Adv. Catal. Relat. Subj., 1970, vol. 21, pp. 323-381.
57. L. Yang and G.R. Belton: Metall. Mater. Trans. B, 1998, vol. 29B, pp. 837–845.
58. Y. Takeda, S. Nakazawa and A. Yazawa: Canadian Metallurgical Quarterly, 1980, vol. 19, pp. 297–305.
59. E.J. Michal and R. Schuhmann: Transactions of the AIME, 1952, vol. 194, pp. 723–728.
60. M. Timuchin and A.E. Morris: Metallurgical Transactions B, 1970, vol. 1B, pp. 3193–3201.
61. S. Hara, T. Araki and K. Ogino: 2nd Int. Symp. on Metallurgical Slags and Fluxes, H.A. Fine and D.R. Gaskell, eds., TMS–AIME, Warrendale, PA, 1984, pp. 441–451.
62. T.H. Wolkenstein: Adv. Catal. Rel. Subj., 1960, vol. XII, pp. 189-264.
63. H. Reiss: J. Phys. Chem., 1985, vol. 89, pp. 3783-3791.
64. H.J. Grabke: 3rd Int. Cong. on Catalysis, 1964, pp. 928–938.
65. H.J. Grabke: Berichte der Bunsen–Gesellschaft – Physical Chemistry, 1965, vol. 69, pp. 48–57.
66. A.W. Cramb, W.R. Graham, and G.R. Belton: Metall. Mater. Trans. B, 1978, vol. 9B, pp. 623–629.
67. G. Trannel: Ph.D. Thesis, University of New South Wales, New South Wales, Australia, 1998.
68. G. Trannel, O. Ostrovski, and S. Jahanshahi: Metall. Mater. Trans. B, 2002, vol. 33B, pp. 61–67.
69. J.A. Duffy: Bonding, Energy levels and Bonds in Inorganic Solids, Longmans, United Kingdom, 1990, p. 161.

Appendix

Table of Experimental Results

Table A.1– The apparent rate constant and the estimated error under various experimental conditions for MnO_x containing slags (the apparent rate constant in ($mol.cm^{-2}.s^{-1}.atm^{-1}$))

'Mn_2O_3' (wt%)	CaO/SiO_2 (mol/mol)	T (K)	CO_2/CO (-)	$K_a \times 10^5$ 1st	$K_a \times 10^5$ 2nd	$K_a \times 10^5$ 3rd	**$K_a \times 10^5$ Avg**	**Error (%)**
10	1.0	1773	10.0	0.196	0.201	0.176	**0.191**	**8**
10	1.0	1773	5.0	0.236	0.297	0.267	**0.267**	**12**
10	1.0	1773	3.0	0.291	0.318	0.300	**0.303**	**5**
10	1.0	1773	1.0	0.582	0.576	0.544	**0.567**	**4**
10	1.0	1773	0.5	0.873	0.872	0.856	**0.867**	**1**
10	1.0	1797	1.0	0.760	0.763	0.749	**0.757**	**1**
10	1.0	1822	1.0	1.05	1.02	1.10	**1.06**	**4**
10	1.0	1845	1.0	1.27	1.25	1.22	**1.24**	**2**
10	1.0	1871	1.0	1.52	1.49	1.49	**1.50**	**1**
20	1.0	1773	10.0	0.194	0.200	0.288	**0.227**	**27**
20	1.0	1773	5.0	0.312	0.313	0.246	**0.290**	**15**
20	1.0	1773	3.0	0.428	0.466	0.420	**0.438**	**6**
20	1.0	1773	1.0	0.773	0.757	0.794	**0.775**	**3**
20	1.0	1773	0.5	1.22	1.14	1.25	**1.20**	**5**
20	1.0	1799	1.0	1.01	1.06	0.968	**1.01**	**5**
20	1.0	1827	1.0	1.18	1.20	1.25	**1.21**	**3**
20	1.0	1849	1.0	1.46	1.44	1.62	**1.51**	**7**
20	1.0	1873	1.0	1.65	1.61	1.71	**1.66**	**3**
30	1.0	1773	10.0	0.224	0.232	0.200	**0.219**	**9**
30	1.0	1773	5.0	0.369	0.354	0.266	**0.329**	**19**
30	1.0	1773	3.0	0.393	0.470	0.397	**0.420**	**12**
30	1.0	1773	1.0	0.808	0.813	0.783	**0.801**	**2**
30	1.0	1773	0.5	1.35	1.47	1.44	**1.42**	**5**

30	1.0	1796	1.0	1.05	1.06	1.01	**1.04**	**2**
30	1.0	1819	1.0	1.32	1.32	1.31	**1.32**	**1**
30	1.0	1842	1.0	1.55	1.57	1.56	**1.56**	**1**
30	1.0	1868	1.0	1.76	1.89	1.76	**1.80**	**5**
30	0.4	1773	10.0	0.313	0.283	0.179	**0.258**	**31**
30	0.4	1773	5.0	0.359	0.299	0.251	**0.303**	**19**
30	0.4	1773	3.0	0.391	0.428	0.448	**0.422**	**7**
30	0.4	1773	1.0	0.755	0.758	0.754	**0.756**	**1**
30	0.4	1773	0.5	1.21	1.32	1.41	**1.31**	**8**
30	0.4	1797	1.0	1.11	1.14	1.14	**1.13**	**2**
30	0.4	1820	1.0	1.30	1.36	1.36	**1.34**	**3**
30	0.4	1844	1.0	1.50	1.57	1.52	**1.53**	**3**
30	0.4	1869	1.0	1.84	1.88	1.89	**1.87**	**2**
30	0.7	1773	10.0	0.219	0.237	0.187	**0.214**	**13**
30	0.7	1773	5.0	0.319	0.350	0.317	**0.329**	**6**
30	0.7	1773	3.0	0.398	0.478	0.474	**0.450**	**12**
30	0.7	1773	1.0	0.742	0.735	0.749	**0.742**	**1**
30	0.7	1773	0.5	1.03	1.17	1.06	**1.09**	**7**
30	0.7	1797	1.0	0.938	0.892	0.876	**0.902**	**4**
30	0.7	1820	1.0	1.17	1.13	1.05	**1.12**	**6**
30	0.7	1844	1.0	1.40	1.36	1.29	**1.35**	**5**
30	0.7	1869	1.0	1.78	1.71	1.71	**1.73**	**3**
30	1.2	1773	10.0	0.271	0.197	0.217	**0.229**	**19**
30	1.2	1773	5.0	0.401	0.403	0.422	**0.409**	**3**
30	1.2	1773	3.0	0.422	0.475	0.465	**0.454**	**7**
30	1.2	1773	1.0	0.803	0.844	0.807	**0.818**	**3**
30	1.2	1773	0.5	1.68	1.55	1.70	**1.64**	**5**
30	1.2	1797	1.0	1.17	1.19	1.19	**1.19**	**1**
30	1.2	1819	1.0	1.40	1.48	1.46	**1.45**	**3**
30	1.2	1844	1.0	1.64	1.66	1.65	**1.65**	**8**
30	1.2	1869	1.0	1.74	1.81	1,80	**1.78**	**3**

40	1.0	1773	10.0	0.205	0.213	0.225	**0.215**	**5**
40	1.0	1773	5.0	0.464	0.378	0.365	**0.402**	**15**
40	1.0	1773	3.0	0.427	0.575	0.470	**0.491**	**17**
40	1.0	1773	1.0	1.17	1.07	1.01	**1.09**	**8**
40	1.0	1773	0.5	1.78	1.74	1.80	**1.77**	**2**
40	1.0	1725	1.0	0.585	0.677	0.778	**0.680**	**14**
40	1.0	1747	1.0	0.862	0.965	0.995	**0.941**	**8**
40	1.0	1798	1.0	1.32	1.23	1.23	**1.26**	**5**
40	1.0	1821	1.0	1.56	1.45	1.46	**1.49**	**5**
40	1.0	1844	1.0	1.64	1.66	1.74	**1.68**	**3**

Table A.2– The apparent rate constant and the estimated error under various experimental conditions for TiO_x containing slags (the apparent rate constant in ($mol.cm^{-2}.s^{-1}.atm^{-1}$))

'TiO_2' (wt%)	CaO/SiO_2 (mol/mol)	T (K)	CO_2/CO (-)	$K_a \times 10^5$ 1st	$K_a \times 10^5$ 2nd	$K_a \times 10^5$ 3rd	**$K_a \times 10^5$ Avg**	**Error (%)**
10	1.0	1773	10.0	0.137	0.075	0.102	**0.105**	**31**
10	1.0	1773	5.0	0.142	0.132	0.140	**0.138**	**4**
10	1.0	1773	3.0	0.163	0.187	0.190	**0.180**	**9**
10	1.0	1773	1.0	0.323	0.349	0.305	**0.326**	**7**
10	1.0	1773	0.5	0.412	0.443	0.417	**0.424**	**4**
10	1.0	1797	1.0	0.471	0.482	0.471	**0.475**	**2**
10	1.0	1821	1.0	0.660	0.639	0.607	**0.635**	**5**
10	1.0	1847	1.0	0.792	0.780	0.775	**0.782**	**1**
10	1.0	1870	1.0	0.942	0.951	0.926	**0.940**	**1**
20	1.0	1773	10.0	0.134	0.092	0.099	**0.108**	**24**
20	1.0	1773	5.0	0.145	0.143	0.142	**0.143**	**1**
20	1.0	1773	3.0	0.190	0.185	0.179	**0.185**	**3**
20	1.0	1773	1.0	0.342	0.338	0.326	**0.335**	**3**
20	1.0	1773	0.5	0.541	0.565	0.514	**0.540**	**5**
20	1.0	1797	1.0	0.482	0.480	0.508	**0.490**	**4**
20	1.0	1820	1.0	0.697	0.684	0.692	**0.691**	**1**
20	1.0	1844	1.0	0.874	0.990	1.08	**0.982**	**11**

20	1.0	1868	1.0	1.09	1.12	1.18	**1.13**	**4**
30	1.0	1773	10.0	0.132	0.085	0.115	**0.111**	**23**
30	1.0	1773	5.0	0.149	0.171	0.174	**0.165**	**10**
30	1.0	1773	3.0	0.196	0.212	0.156	**0.188**	**17**
30	1.0	1773	1.0	0.357	0.373	0.349	**0.360**	**4**
30	1.0	1773	0.5	0.542	0.534	0.550	**0.542**	**2**
30	1.0	1797	1.0	0.492	0.506	0.349	**0.360**	**2**
30	1.0	1820	1.0	0.648	0.642	0.656	**0.649**	**1**
30	1.0	1844	1.0	0.819	0.827	0.831	**0.826**	**1**
30	1.0	1868	1.0	1.03	0.984	1.02	**1.01**	**2**
30	0.8	1773	10.0	0.111	0.104	0.096	**0.104**	**7**
30	0.8	1773	5.0	0.149	0.145	0.151	**0.148**	**2**
30	0.8	1773	3.0	0.186	0.170	0.179	**0.178**	**5**
30	0.8	1773	1.0	0.327	0.352	0.353	**0.344**	**5**
30	0.8	1773	0.5	0.510	0.455	0.478	**0.481**	**6**
30	0.8	1796	1.0	0.464	0.506	0.574	**0.515**	**12**
30	0.8	1820	1.0	0.668	0.654	0.703	**0.675**	**4**
30	0.8	1842	1.0	0.861	0.825	0.821	**0.836**	**3**
30	0.8	1866	1.0	1.02	1.04	1.03	**1.03**	**1**
30	1.2	1773	10.0	0.157	0.137	0.101	**0.131**	**24**
30	1.2	1773	5.0	0.195	0.196	0.155	**0.182**	**15**
30	1.2	1773	3.0	0.205	0.240	0.183	**0.209**	**15**
30	1.2	1773	1.0	0.588	0.470	0.494	**0.517**	**14**
30	1.2	1773	0.5	0.712	0.670	0.863	**0.748**	**15**
30	1.2	1796	1.0	0.798	0.781	0.782	**0.787**	**1**
30	1.2	1822	1.0	0.815	0.967	0.929	**0.904**	**10**
30	1.2	1846	1.0	1.14	1.13	1.15	**1.14**	**1**
30	1.2	1866	1.0	1.36	1.35	1.38	**1.36**	**1**
40	1.0	1773	10.0	0.127	0.100	0.104	**0.110**	**16**
40	1.0	1773	5.0	0.168	0.187	0.156	**0.170**	**10**
40	1.0	1773	3.0	0.219	0.237	0.224	**0.227**	**5**
40	1.0	1773	1.0	0.466	0.379	0.443	**0.429**	**12**

40	1.0	1773	0.5	0.602	0.606	0.598	**0.602**	**1**
40	1.0	1796	1.0	0.567	0.559	0.542	**0.556**	**3**
40	1.0	1820	1.0	0.722	0.720	0.726	**0.723**	**1**
40	1.0	1842	1.0	0.934	0.903	0.920	**0.919**	**2**
40	1.0	1866	1.0	1.12	1.10	1.13	**1.12**	**2**
50	1.0	1773	10.0	0.105	0.110	0.131	**0.115**	**14**
50	1.0	1773	5.0	0.195	0.228	0.208	**0.210**	**9**
50	1.0	1773	3.0	0.247	0.256	0.272	**0.258**	**5**
50	1.0	1773	1.0	0.477	0.417	0.462	**0.452**	**8**
50	1.0	1773	0.5	0.752	0.677	0.689	**0.706**	**7**
50	1.0	1796	1.0	0.655	0.593	0.694	**0.647**	**8**
50	1.0	1820	1.0	0.792	0.783	0.842	**0.806**	**4**
50	1.0	1842	1.0	1.07	1.04	1.04	**1.05**	**2**
50	1.0	1866	1.0	1.20	1.25	1.26	**1.24**	**3**